MIT Libraries | DSpace@MIT

MIT Open Access Articles

Genome-scale screens identify factors regulating tumor cell responses to natural killer cells

The MIT Faculty has made this article openly available. ***Please share*** how this access benefits you. Your story matters.

Citation: Sheffer, Michal et al. "Genome-scale screens identify factors regulating tumor cell responses to natural killer cells." Nature Genetics 53, 8 (July 2021): 1196–1206. © 2021 The Author(s)

As Published: http://dx.doi.org/10.1038/s41588-021-00889-w

Publisher: Springer Science and Business Media LLC

Persistent URL: https://hdl.handle.net/1721.1/131260

Version: Author's final manuscript: final author's manuscript post peer review, without publisher's formatting or copy editing

Terms of Use: Article is made available in accordance with the publisher's policy and may be subject to US copyright law. Please refer to the publisher's site for terms of use.

Massachusetts Institute of Technology

1. Extended Data

Figure #	Figure title One sentence only	Filename This should be the name the file is saved as when it is uploaded to our system. Please include the file extension. i.e.: *Smith_ED_Fig1.jpg*	Figure Legend If you are citing a reference for the first time in these legends, please include all new references in the Online Methods References section, and carry on the numbering from the main References section of the paper.
Extended Data Fig. 1	**Genes associated with tumour cell responses to NK cells in PRISM studies**	extended data 1-01.jpg	**Extended Data 1. Genes associated with tumour cell responses to NK cells in PRISM studies** **a,** Scatter plots for AUC derived from PRISM study per time point (x-axis) and from cytotoxic assays of individual cell lines (y-axis). The Spearman correlation coefficients are specified for each time point. **b,** Volcano plot for the $-\log_{10}$(p-value) of the Spearman correlation between AUC and gene expression (y-axis) vs $\log_2$ fold changes of expression for the respective genes between NK cell-resistant (upper third of AUC distribution) and NK cell-sensitive (lower third of AUC distribution) cell lines (see Methods). Results are shown for 24hr-AUC as representative of results for other time points. Genes with sgRNA enrichment are labeled red and sgRNA depletion are labeled blue. Genes in bold were significant based on MaGECK and STARS analyses in at least one CRISPR screen.
Extended Data Fig. 2	**Key regulators of tumor cell responses to NK cells in CRISPR studies**	extended data 2-01.jpg	**Extended Data 2. Key regulators of tumour cell responses to NK cells in CRISPR studies** Plots for sgRNA enrichment (upper panels) or depletion (lower panels) for each one of the genome-scale CRISPR gene-editing screens. Highlighted genes were identified as significant based on MaGECK and STARS in at least one screen.
Extended Data Fig. 3	**Stratified PRISM-based analyses for global (all cell**	extended data 3-01.jpg	**Extended Data 3. Stratified PRISM-based analyses for global (all cell lines), epithelial-like or mesenchymal-like groups of lines.**

	lines), epithelial-like or mesenchymal-like groups of lines		Normalized transcript levels for genes which have significant correlation (Spearman correlation coefficient, adjusted p-values<0.05, see Methods) with AUC values in ≥2 time points for the entire set of PRISM cell lines. A gene was considered to correlate with AUC in the epithelial-like or the mesenchymal-like subset of lines if p-value ≤0.05 in ≥2 time points in the respective subgroup analysis. Horizontal black lines represent genes which exhibited significant sgRNA enrichment or depletion in at least one of the CRISPR studies (based on MAGECK and STARS) and in a manner concordant with the results of the PRISM analyses. Group A was enriched for these genes, compared with groups B-D (p=0.022, χ^2 test, df=1).
Extended Data Fig. 4	**Integration of results for PRISM and CRISPR-based identification of regulators of tumor cell response to NK cells**	extended data 4-01.jpg	**Extended Data 4. Integration of results for PRISM and CRISPR-based identification of regulators of tumour cell response to NK cells** Functional clusters of genes that were associated with tumour cell responses to NK cells (based on genes that were significant for both MaGECK and STARS in at least one screen). Gene highlighted in bold were also significant for PRISM.
Extended Data Fig. 5	**B7-H6 and HLA-E as key regulators of NK cell responses**	extended data 5-01.jpg	**Extended Data 5. B7-H6 and HLA-E as key regulators of NK cell responses** **a,** *In vivo* testing of NK cell activity against SW620 tumour cells with vs. without *B7-H6* CRISPR knockout: Bioluminescence intensity (photons/sec/cm^2) measured at week 2. P-values are calculated using two- sided Mann-Whitney tests between B7-H6$^-$ vs. B7-H6+ tumours in each group. Data are represented as mean ± SD, n=10 per group. **b,** *B7-H6* log2-fold changes of tumour vs. normal samples in RNA-seq data of the TCGA dataset. Data are represented as box/dot plots, demarcating the first and third quartiles of the distribution, with the median shown in the center and whiskers covering data within 1.5x the interquartile range of the box (significant FDR-adjusted p-values for upregulation are

			shown in red; two-sided Mann-Whitney tests). **c,** Heatmap for z-scores of transcript levels for antigen presentation genes, showing co-expression in the different cancer types of the TCGA. The gene expression levels were normalized across the samples of each cancer type. **d,** Western blot analyses for STAT1 protein levels in *STAT1* knockouts vs. *OR10A2* as control knockouts in HT29 and SW620 cell lines. Staining for GAPDH on the same uncropped membrane serves as loading control. n=2 distinct experiments. **e,** Flow cytometry analysis for surface HLA-E levels in HT29 cells with sgRNA for *HLA-E* vs. control sgRNA with vs. without IFNγ (5ng/ml) over-night incubation, n=2 experiments.
Extended Data Fig. 6	**Functional relationship of B7-H6 and MHC class I molecules**	extended data 6-01.jpg	**Extended Data 6. Functional relationship of B7-H6 and MHC class I molecules.** **a,** Comparison of transcript levels between Wild-Type (WT) and *B2M*-mutated cell lines of the PRISM collection (coding mutations), Mann-Whitney two-sided test. **b,** Spearman correlation coefficients between *B7-H6* and *B2M* (upper panel) or *HLA-E* (lower panel) in TCGA and CCLE datasets. **c,** Heatmap of the expression levels of *B7-H6* and *HLA-E* in PRISM cell lines sorted based on difference (log_2 fold) of *B7-H6* compared with *HLA-E*. **d,** Percentages of MSI cell lines (brown) vs. MSS cell lines (orange) in the group of HLA-low (n=35) cell lines compared with all other lines (n=348) of the PRISM-based surface proteomic analysis. **e,** HLA-A/B/C surface protein scores or *B2M* transcript levels between the groups of MSS vs. MSI cell lines; two-sided Mann-Whitney test. **f,** Left: AUC for MSI lines with low-HLA-A/B/C (n=13) vs. all other lines (n=370) of the PRISM-based surface proteomic analysis. Right: AUC for MSI lines with low *B2M* expression (n=37) vs. all other

			lines (n=490); two-sided Mann-Whitney test. Results are shown for 24hr-AUC and are representative of those for other time points. **g,** *HLA-E* and *B2M* $\log_2$-fold changes of tumour vs. normal samples in the RNA-seq data of the TCGA dataset (significant FDR-adjusted p-values for downregulation are shown in red; two-sided Mann-Whitney). Data in **a,e,f,g,** are represented as box/dot plots, demarcating the first and third quartiles of the distribution, with the median shown in the center and whiskers covering data within 1.5x the interquartile range of the box.
Extended Data Fig. 7	**Transcriptional signatures in tumor cells associated with responses to NK cells**	extended data 7-01.jpg	**Extended Data 7. Tumour cell transcriptional signatures associated with responses to NK cells.** **a,** Left: GSEA NES scores for selected gene sets that had FDR adjusted p<0.05 in at least two time points in analyses that included all PRISM cell lines: NES are also shown for GSEA of only epithelial-like and only mesenchymal-like lines (see Methods). Right: GSEA NES scores for same gene sets as in left panel in ICI non-responders vs. responders (see Methods). Red and blue represent enrichment and suppression, respectively, of gene sets in the corresponding analyses. Lack of significant changes (p>0.05) was colored white. **b-c**, Normalized expression levels of core genes from pathways correlating with AUC (see Methods) in **b,** epithelial-like or mesenchymal-like cell lines and **c**, TCGA tumours, sorted by the expression of *CDH1* and *ZEB2* using SPIN[40]. Tumours with low vs. high *CDH1* are separated with a dotted line. **d**, SW620 cells were pre-treated for 12 hrs with 50nM of the HDAC inhibitor panobinostat, 5 ng/ml IFNγ or DMSO. The cells were stained with anti-HLA-E (left) and anti-B7-H6 (right) antibodies. Unlabeled controls are colored grey. n=1 experiments. **e**, Flow cytometry assays to quantify NK

			cell cytotoxicity against tumour cells (see Methods) pre-treated with HDAC inhibitor or DMSO. Cells were treated with 12.5nM panobinostat and cocultured with NK cells in two E:T ratios. n=4 distinct experiments. **f**, GSEA enrichment plots for select gene sets from **a,** in all cell lines of PRISM (upper) and in ICI non-responders vs. responders of the Riaz *et al.* dataset (lower). **g**, Gene scores for NK cell sensitivity in ICI non-responders vs. responders of the Riaz *et al*. dataset (see Methods, two-sided Mann-Whitney test).

2. Supplementary Information:

A. Flat Files

Item	**Present?**	**Filename** **This should be the name the file is saved as when it is uploaded to our system, and should include the file extension. The extension must be .pdf**	**A brief, numerical description of file contents.** **i.e.: *Supplementary Figures 1-4, Supplementary Discussion, and Supplementary Tables 1-4.***
Supplementary Information	Yes	Supplementary Info.pdf	Supplementary Methods, Supplementary Tables 2,6,7.
Reporting Summary	Yes	Reporting-summary.pdf	
Peer Review	No	N/A	

B. Additional Supplementary Files

Type	**Number** **If there are multiple files of the same type this should be the numerical indicator. i.e. "1" for Video 1, "2" for Video 2, etc.**	**Filename** **This should be the name the file is saved as when it is uploaded to our system, and should include the file extension. i.e.: *Smith_***	**Legend or Descriptive Caption** **Describe the contents of the file**

		Supplementary_Video_1.mov	
Supplementary Table	1	Supplementary_Tables.xlsx	Supplementary Tables 1, 3-5

3. Source Data

Figure	**Filename** **This should be the name the file is saved as when it is uploaded to our system, and should include the file extension. i.e.:** ***Smith_SourceData_Fig1.xls,*** **or** ***Smith_ Unmodified_Gels_Fig1.pdf***	**Data description** **i.e.: Unprocessed Western Blots and/or gels, Statistical Source Data, etc.**
Source Data Extended Data Fig. 1		
Source Data Extended Data Fig. 2		
Source Data Extended Data Fig. 3		
Source Data Extended Data Fig. 4		
Source Data Extended Data Fig. 5	Source_data_1_STAT1_blot_30 sec.jpg	Unprocessed western blot

Genome-scale screens identify factors regulating tumour cell responses to natural killer cells

Michal Sheffer*[1,2,3,4], Emily Lowry[1], Nicky Beelen[5,6], Minasri Borah[1], Suha Naffar-Abu Amara[7], Chris C. Mader[3], Jennifer A. Roth[3], Aviad Tsherniak[3], Samuel S. Freeman[3], Olga Dashevsky[1,2,3,4], Sara Gandolfi[1,2,3,4], Samantha Bender[3], Jordan G. Bryan[3,] Cong Zhu[3], Li Wang[3], Ifrah Tariq[3,8], Govinda M. Kamath[9], Ricardo De Matos Simoes[1,2,3,4], Eugen Dhimolea[1,2,3,4], Channing Yu[1,2,3], Yiguo Hu[1#], Olli Dufva[10,11,12], Marios Giannakis[1,2,3], Vasilis Syrgkanis[9], Ernest Fraenkel[3,8], Todd Golub[1,3], Rizwan Romee[1,2], Satu Mustjoki[10,11,12], Aedin C. Culhane[13,14], Lotte Wieten[5,6] and Constantine S. Mitsiades*[1,2,3,4]

1. Department of Medical Oncology, Dana-Farber Cancer Institute, Boston, MA, USA
2. Department of Medicine, Harvard Medical School, Boston, MA, USA
3. Broad Institute of Massachusetts Institute of Technology (MIT) and Harvard, Cambridge, MA, USA.
4. Ludwig Center, Harvard Medical School, Boston, MA, USA
5. Department of Transplantation Immunology, Maastricht University Medical Center+, Maastricht, The Netherlands
6. School for Oncology and Developmental Biology, Maastricht University Medical Center+ GROW, Maastricht, The Netherlands
7. Department of Cell Biology, Harvard Medical School, Boston, MA, USA
8. Department of Biological Engineering, Massachusetts Institute of Technology, Cambridge, MA, USA
9. Microsoft Research, Cambridge, MA, USA
10. Hematology Research Unit Helsinki, Helsinki University Hospital Comprehensive Cancer Center, Helsinki, Finland
11. Translational Immunology Research Program and Department of Clinical Chemistry and Hematology, University of Helsinki, Helsinki, Finland
12. iCAN Digital Precision Cancer Medicine Flagship, Helsinki, Finland.
13. Department of Data Science, Dana-Farber Cancer Institute, Boston MA, USA
14. Department of Biostatistics, Harvard TH Chan School of Public Health, Boston, MA, USA

(# present address: Sichuan University, Chengdu, China).

Correspondence: Michal_Sheffer@dfci.havard.edu and Constantine_Mitsiades@dfci.harvard.edu

Abstract

To systematically define molecular features in human tumour cells which determine their degree of sensitivity to human allogeneic natural killer (NK) cells, we quantified the NK cell responsiveness of hundreds of molecularly-annotated “DNA-barcoded” solid tumour cell lines in multiplexed format and applied genome-scale CRISPR-based gene editing screens in several solid tumour cell lines to functionally interrogate which genes in tumour cells regulate the response to NK cells. In these orthogonal studies, NK-sensitive tumour cells tend to exhibit “mesenchymal-like” transcriptional programs; high transcriptional signature for chromatin

remodeling complexes; high levels of *B7-H6* (*NCR3LG1*); low levels of *HLA-E/*antigen presentation genes. Importantly, transcriptional signatures of NK cell-sensitive tumour cells correlate with immune checkpoint inhibitor (ICI) resistance in clinical samples. This study provides a comprehensive map of mechanisms regulating tumour cell responses to NK cells, with implications for future biomarker-driven applications of NK cell immunotherapies.

Introduction

Clinical and preclinical studies have documented that infusions of allogeneic NK cells can be safely performed across Human Leukocyte Antigen (HLA) barriers and avoid the graft-versus-host reactions that are an inherent challenge for immunotherapies based on administration of allogeneic T cells[1-4]. The long-standing interest in potential anti-cancer therapeutic applications of NK cells has recently increased, reflecting a hope that these cells may successfully target tumours with primary or secondary resistance to immune checkpoint inhibitors and T-cell-based immunotherapies[5,6].

We thus sought to systematically examine which molecular features in human tumour cells determine their degree of sensitivity to human allogeneic NK cells and confirm whether these mechanisms are broadly generalizable to genotypically-diverse types of tumours. Towards this goal, we leveraged the high-throughput capabilities of two distinct platforms, namely the PRISM (Profiling Relative Inhibition Simultaneously in Mixtures) approach[7] to simultaneously examine the NK cell responsiveness of several hundreds of molecularly-annotated "DNA-barcoded" solid tumour cell lines in a multiplexed format; and clustered regularly interspaced short palindromic repeats (CRISPR)-based gene editing approaches[8-10], to examine at genome-scale which genes regulate the response vs. resistance of several solid tumour cell lines to NK cells.

Results

PRISM and CRISPR screens in NK cell-treated tumor lines

PRISM pools of solid tumour cell lines, each with a distinct "DNA barcode", were exposed to freshly-isolated healthy donor-derived NK cells at different time points and effector-to-tumour (E:T) ratios to quantify their response to the cytotoxic effect of NK cells (Fig. 1a). Area under the curve (AUC) for relative tumour cell viability across E:T ratios was calculated per cell line and time point (Fig. 1a,b, Supplementary Table 1). Selected lines with high vs. low AUC (i.e. NK cell-resistant vs. -sensitive, Fig. 1b,c) were examined individually (non-pooled assays), yielding

results concordant with the pooled PRISM studies (Extended Data 1a, Supplementary Table 2). The ranked list of AUCs was correlated with transcript levels and other profiles generated by the Cancer Cell Line Encyclopedia (CCLE)[11] of each gene in univariate analyses (Extended Data 1b and Supplementary Table 3).

To complement the PRISM studies, we performed genome-scale CRISPR gene editing screens on colorectal cell lines with various NK cell sensitivities; HCT15, SW620 and HT29 (Fig. 2a,b) were cultured alone vs. treated with *ex vivo* expanded NK cells from different donors. We identified genes whose sgRNA-mediated knockouts were enriched or depleted in tumour cells that survived the NK cell treatment, compared with untreated controls (Extended Data 2, Supplementary Table 4). We placed emphasis on genes associated with NK cell sensitivity that have negative correlation of their transcript levels (RNA sequencing [RNAseq]) with AUC (calculated separately for each time-point) and sgRNA enrichment in at least one CRISPR screen; and genes associated with resistance have positive correlation of their transcript levels with AUC and sgRNA depletion in at least one CRISPR screen. These genes are highlighted in Extended Data 1b.

Responses of mesenchymal- vs. epithelial-like tumour cells

Principal component analyses (PCA; Fig. 3a) of proteomic and transcriptional profiles identified in an unbiased manner two main clusters of cell lines which exhibited epithelial-like (e.g. *CDH1* expression) vs. mesenchymal-like (e.g. *VIM*, *ZEB1*, *ZEB2* expression) characteristics: these two clusters also exhibited differential expression for the large majority of genes (Fig. 3b-d) and, importantly, higher vs. lower average AUCs, respectively (Fig. 3b). The distributions of AUCs across individual tumour types overlap extensively but sorting according to median AUCs reveals that tumour types highly enriched for “mesenchymal-like” cell lines tend to be over-represented among those with lower median AUCs (Fig. 3e). Notably, even cell lines derived from tumours generally considered to be of epithelial origin may exhibit “mesenchymal-like” transcriptional signature and therefore more likely to respond to NK cells. We tested this assumption on two different clones from the same patient-derived ovarian tumour that exhibited, respectively, epithelial-like (low *VIM* [vimentin], high *CDH1* [E-cadherin]) vs. mesenchymal-like (high *VIM*, low *CDH1*) transcriptional features and found that the latter was indeed more sensitive to NK cells cytotoxicity (Fig. 3f).

To control for the strong influence of the epithelial-like vs. mesenchymal-like state on both the molecular features of PRISM cell lines and their responses to NK cells, we complemented our PRISM analysis correlating gene expression data with AUCs across all PRISM cell lines (global

analysis), with similar stratified analyses focused on only epithelial-like or only mesenchymal-like cell lines (Extended Data 3 and Supplementary Table 5). Genes correlating with AUCs in all stratifications (Group A) were more enriched for genes also identified in a functionally concordant manner in at least one CRISPR screen, suggesting a lineage-agnostic role of these genes in regulating tumour cell responses to NK cells (p=0.022, χ^2 test, df=1).

Integration of PRISM, CRISPR and molecular profiling data

The integration of PRISM and CRISPR studies identified genes whose transcript levels correlate with AUCs across all PRISM cell lines (and, for most of these genes, also in either or both stratified analyses within epithelial-like or mesenchymal-like cell lines; Extended Data 3 and Supplementary Table 5) and which are also concordantly identified as regulators of NK cell response in at least two (Fig. 4a,b) or one of our CRISPR screens. Additional genes were identified by CRISPR to be functionally linked to regulation of tumour cell responses to NK cells, without correlation of their transcript levels with AUC (Extended Data 4). We did not identify any individual genes whose mutation status associated with AUCs after adjusting for multiplicity of testing, though mutations in a few genes had significant nominal p-values for association with lower (e.g., *PTPN13*, *B2M* and *MET*) or higher (e.g. *CDKN2A and KRAS*) AUCs.

The genes identified through integration of PRISM and CRISPR results define a comprehensive landscape of regulators, including known and previously understudied genes. The most consistent positive regulator of response to NK cells was *B7-H6* (an activating ligand for the NK receptor *NCR3* [*NKp30*][12,13]), the only gene with significant sgRNA enrichment in all CRISPR screens and negative correlation of transcript levels with AUCs across PRISM cell lines (Fig. 4a,b, Extended Data 2, Supplementary Table 4,5). Other known activating ligands for NK cells did not exhibit consistent sgRNA enrichment across CRISPR screens. Additional positive regulators of response to NK cells included chromatin remodeling regulators (e.g. *RBBP4*, *ARID1A*); *BAG2 (*member of the same family as the *NCR3* ligand BAG6*);* and regulators of apoptosis (e.g. *CASP7*, *BAX* and *DFFA*).

Prominent negative regulators of response to NK cells include the NK-inhibitory ligand *HLA-E*, a non-classical major histocompatibility complex (MHC) class I molecule that binds the NK inhibitory receptor *KLRC1* (NKG2A*)* [14-16]; classical MHC class I genes (e.g., *HLA-C*, with less pronounced quantitative metrics in CRISPR studies than *HLA-E*); and genes involved in MHC class I molecules' surface expression (e.g. antigen presentation machinery genes, e.g. *B2M, TAP1, TAP2, and TAPBP*) or transcriptional regulation, including receptors (e.g. *IFNGR1*, *IFNGR2*), effectors (e.g. *STAT1*) and regulators of Interferon-gamma (IFNγ) signaling. Other

notable genes associated with NK cell resistance in PRISM and/or CRISPR data included the epithelial markers E-Cadherin (*CDH1)* and *CLDN7*; the Polycomb-related gene *MBTD1*; diverse genes involved in amino-sugar metabolism and regulation of protein glycosylation (e.g. *GALE*, which regulates the expression of immunoregulatory Siglec ligands)*;* and the Ras-related genes *SSFA2 (a KRAS*-induced actin-interacting protein*)* and *RHOV* (an atypical Rho GTPase member of the *RAS* homolog family).

B7-H6 promotes NK-sensitivity *in vitro* and *in vivo*

As *B7-H6* was the most prominent gene associated with pronounced NK cell sensitivity, we further examined its functional role. *In vitro* cytotoxicity of primary NK cells is decreased against different cell lines with *B7-H6* knockout (*sgB7-H6*) compared with respective controls (*sgCtrl*). (Fig. 4c,d). Surface expression of *B7-H6* protein is heterogeneous in HT29 cells and their exposure to NK cells led to dose-dependent decrease in relative abundance of *B7-H6*$^{+}$ cells (Fig. 4e). We tested the *in vivo* role of *B7-H6 in* immunocompromised NSG mice receiving contralateral subcutaneous flank injections of SW620 cells with vs. without knockout of *B7-H6*, respectively. Control mice were injected only with tumour cells, while the treatment group were injected with a mix of NK cells and tumour cells (Fig. 4f). Tumour growth was observed for NK cell-exposed *sgB7-H6* tumours while their *sgCtrl* counterparts were undetectable or much smaller in size (Fig. 4g,h, Extended Data 5a). *B7-H6* transcript is highly expressed in kidney chromophobe, stomach, colorectal and breast cancers compared with their respective normal tissues (TCGA data, Extended Data 5b) suggesting that NK cell-based therapies targeting B7-H6 may be especially relevant to subsets of patients from these tumour types.

HLA-E suppresses NK-sensitivity of tumor cells

Antigen presentation pathway genes, including MHC class I molecules, are tightly co-regulated by IFNγ-induced JAK/STAT signaling[17], and are highly correlated across the TCGA dataset (Extended Data 5c). Among MHC class I genes, *HLA-E* had the most pronounced sgRNA depletion (i.e. sensitization to NK cells) in *B2M*-proficient SW620 and HT29 cells (Fig. 5a). We hypothesized that *HLA-E* is a key determinant of NK cell resistance among MHC class I/antigen presentation machinery genes. Towards this hypothesis, we observed that both HLA-E and HLA-A/B/C are expressed (although at considerably higher levels for the latter) in the absence of IFNγ and are further induced by IFNγ; and this induction is abrogated by knockout of *STAT1* (Fig. 5b). Tumour cells with knockout of *STAT1* or *HLA-E* have increased NK cell sensitivity

(Fig. 5c, Extended Data 5d,e) despite expression of classical MHC class I molecules, suggesting that these changes in NK cell responsiveness are primarily due to lack of HLA-E.

Functional relationship of B7-H6 and MHC class I molecules

To examine relationships between B7-H6 and MHC class I molecules at the transcript and surface expression levels, the pool of PRISM cell lines was processed for fluorescence-activated cell sorting (FACS) into sub-populations with different surface expression for these proteins and sequencing read counts for their respective "barcodes" were converted into surface expression protein scores (Fig. 6a, Methods). Surface protein scores for B7-H6 and HLA-A/B/C exhibited their highest correlation with transcript levels for *B7-H6* and *B2M*, respectively (Fig 6b,c). *B2M* transcript levels may be viewed as a surrogate for surface expression of MHC class I complex, which is lost in *B2M*-mutated lines. Indeed, *B2M*-mutated lines have lower levels of *B2M* transcript but not HLA transcripts (Extended Data 6a). High protein scores for B7-H6, low for HLA-A/B/C are associated with low AUCs. Interestingly, the overlap between these two groups was significant (Fig 6d). CCLE and TCGA data indicate negative correlation between transcript levels of *B7-H6* and *B2M* or *HLA-E*, with association to NK cells cytotoxicity in PRISM (Extended Data 6b,c). In addition, low surface HLA-A/B/C expression is enriched for Microsatellite Instability (MSI) lines, which exhibit lower *B2M* transcript levels and lower AUCs (Extended Data 6d-f). Collectively, these observations suggest that MSI tumours with low *B2M* expression levels may be highly sensitive to NK cells. We consider that MSI state/high tumour mutational burden does not necessarily predict by itself whether a given cell line is more likely to be NK cell-sensitive, as the effect of tumour mutational burden may depend on which specific genes are mutated: if these mutations involve *B2M* / antigen presentation machinery genes, MSI status may be associated with NK cell sensitivity. Downregulation of MHC class I transcripts is common among certain cancer types compared to their respective normal tissues (TCGA dataset, Extended Data 6g), with colorectal cancer as prominent example, which also exhibit up-regulation of *B7-H6*.

Functional link of chromatin remodeling and NK-sensitivity

Building on our gene-level studies, we examined the molecular determinants of tumour cell responses to NK cells at the gene-set/pathway levels. Gene set enrichment analysis (GSEA; Extended Data 7a, Left) indicated that genes associated with NK cell resistance were enriched for epithelial-like gene signatures, antigen presentation machinery genes and its related pathways (e.g. signatures for graft-versus-host disease and MHC genes), consistent with the

sgRNA depletion of MHC class I genes in our CRISPR studies. Conversely, genes associated with NK cell sensitivity were enriched for mesenchymal-like gene signatures and chromatin remodeling complexes (HDAC, SWI/SNF and Polycomb), consistent with the sgRNA enrichment for *RBBP4*, *ARID1A* in our CRISPR studies. This association of AUCs with *B7-H6,* genes of the GSEA enrichment core for chromatin remodeling and antigen presentation signatures was confirmed in analyses including all PRISM cell lines (Fig. 7a) and in stratified analyses including only epithelial-like or mesenchymal-like lines (Extended Data 7b). In addition, analysis of TCGA transcript levels reveals that tumours of mesenchymal origin express lower levels of antigen presentation genes and IFNγ response genes compared with tumours of epithelial origin (Extended Data 7c), suggesting a link between epithelial-like transcriptional signatures and antigen presentation or IFNγ response levels. The inverse correlation between chromatin remodeling genes and *HLA-E* or the positive correlation of *HLA-E* with antigen presentation genes, was observed in all tumour types of the TCGA dataset that we examined (Fig. 7b). Based on these observations, we further examined how perturbation of chromatin remodeling may affect the expression of antigen presentation genes and tumour cell response to NK cells. Indeed, these signatures are reversed in cell lines treated with various broad spectrum HDAC inhibitors[18-20] (Fig. 7c) and knockouts of several chromatin remodeling genes leads to increased surface expression of MHC class I levels in CRISPR studies in K562 leukemia cells[21] (Fig. 7d). Importantly, pre-treatment of SW620 cells with HDAC inhibitor led to STAT1-independent upregulation of HLA-E; downregulation of B7-H6; and decreased sensitivity to NK cells (Extended Data 7d,e).

ICI resistance correlates with NK sensitivity signature

Loss of MHC class I molecules in tumour cells confers increased sensitivity to NK cells (e.g. Fig. 4a,b), but has been implicated in resistance to immune checkpoint inhibition (ICI)[5,6]. Interestingly, our PRISM studies indicate that tumour cells with mesenchymal-like transcriptional program tend to be more sensitive to NK cells. Consistent with this observation, among mesenchymal tumours, most types of soft-tissue sarcomas tend to exhibit limited, if any, clinical response to ICI treatment, with the notable exception of undifferentiated pleomorphic sarcoma (UPS), which is over-represented within soft-tissue sarcomas that respond to ICI[22,23]. Given these considerations, we hypothesized that the broader collection of transcriptional signatures associated with NK cell responsiveness may correlate with decreased response to ICI. We addressed this hypothesis by comparing transcriptional profiles of tumour samples from non-responders vs. responders from five cohorts of ICI-treated melanoma patients[24-28]; and tumours

of patients with Leiomyosarcoma (LMS) vs. UPS. In both settings (Fig. 7e,f, Fig. 8a-c and Extended Data 7a right panel, f), transcriptional signatures associated with NK cell sensitivity are enriched in samples of patients who do not respond to ICI. Indeed, the transcriptional signature of genes defined by PRISM and CRISPR to be associated with NK sensitivity, as well as mesenchymal-like and chromatin remodeling signatures were upregulated, while transcriptional signatures associated with NK cell resistance, including epithelial-like and antigen presentation machinery genes were downregulated in ICI non-responders compared with ICI responders (Fig. 7e, Fig. 8a,b and Extended Data 7a right panel, f). Furthermore, analysis of patient-based NK-sensitivity gene score for these genes indicated significant difference for non-responders vs. responders (Extended Data 7g). Consistent with these results, the group of genes associated with NK resistance exhibited positive enrichment in UPS compared with LMS tumours in TCGA, while the NK sensitivity gene set had negative enrichment (Fig. 7f, Fig. 8c). Collectively, these observations suggest that molecular signatures of resistance to other forms of immunotherapy do not necessarily correlate with resistance to NK cells and may even be associated with increased responsiveness to NK cells.

Discussion

Understanding which molecular pathways regulate the activity of NK cells against large genotypically-diverse cohorts of human tumour cells is important for any efforts to “personalize” NK cell-based therapeutic approaches. We addressed this question through the orthogonal use of PRISM phenotypic screens and CRISPR gene-editing studies. PRISM enables multiplexed quantification of treatment responses across hundreds of “DNA-barcoded” cell lines. Our study thus comprehensively correlates the molecular features of large numbers of tumor cells with their response to uniform preclinical administration of a cell-based immunotherapy, at a scale that would logistically be challenging to achieve in clinical settings. CRISPR screens provide direct functional evidence of which gene perturbations influence treatment responsiveness in each individual cell line. This orthogonal use of PRISM and CRISPR provided an integrated “multi-omic” and functional genomics profile of a “typical” NK cell-sensitive tumour cell: although mechanisms in tumour cells that regulate their response to NK cells are multifactorial and appear to involve the aggregate impact of several parameters, cell lines more responsive to NK cells tend to have a “mesenchymal-like” transcriptional program; high levels of B7-H6 and transcriptional signatures for chromatin regulatory complexes (e.g. HDAC/Polycomb/BAF); and low levels of MHC class I molecules, especially HLA-E, and transcriptional signatures for

antigen presentation machinery genes and IFNγ signaling. Two or more of these features often co-exist in NK cell-sensitive tumour cell lines (Fig. 8d).

The mechanistic basis of the differential average NK cell sensitivity between mesenchymal-like vs. epithelial-like cell lines is likely multifactorial. Epithelial-like tumour cell lines exhibited on average, compared to mesenchymal-like lines, lower levels of transcriptional signatures for chromatin remodeling genes and higher levels for transcriptional signature for antigen presentation / MHC class I molecules. Our study also identified several genes (e.g. *CDH1*, a known ligand for the inhibitory NK receptor *KLRG1*[29], and *CLDN7*) which exhibit (i) positive correlation of their transcript levels with high AUC (lower sensitivity) in global analysis of all PRISM cell lines; (ii) higher transcript levels in epithelial-like (compared to mesenchymal-like) lines and (iii) sgRNAs depletion in at least one of our CRISPR studies, indicating that these latter genes can be considered plausible mediators, at least partly, of the lower average sensitivity of epithelial-like cell lines. In contrast, perturbation of several other genes differentially expressed between mesenchymal vs. epithelial-like lines (e.g. *VIM* or *CDH2*; data not shown) did not alter NK cell responsiveness. The differential average NK cell-sensitivity between mesenchymal- vs. epithelial-like tumour cells prompted us to perform stratified PRISM-based correlative analyses within each of these two clusters: this validated that top genes/pathways identified from our PRISM-CRISPR studies (including B7-H6, HLA-E or transcriptional signatures for HLA-class I/antigen presentation machinery or chromatin remodeling genes) remained associated with the extent of NK cell response within both clusters of tumor cells; but also provided a blueprint for prospective studies of markers with preferential role in either mesenchymal or epithelial tumours.

B7-H6 is a known ligand for the NK cell-activation receptor NCR3 (NKp30), yet its role in regulating tumour cell responses to NK cells is under-studied. This may partly reflect the fact that most rodent models frequently used in tumour immunology studies lack a close homologue to the human *B7-H6*[12,13], which may explain why this gene was not identified in functional studies using a mouse melanoma cell line[30]. *B7-H6* inversely correlates with MHC class I molecules, at both transcript and surface protein levels. Nevertheless, the role of B7-H6 on tumour cell sensitivity to NK cells is functionally independent of MHC class I molecules, as knockout of *B7-H6* decreases tumour cell response to NK cells both in MHC class I-proficient cell lines (without affecting HLA-E expression) and -deficient lines. Two recent studies[21,31] identify *B7-H6* as a “hit” in CRISPR knockout screens on NK cell-treated K562 leukaemia cells,

a main target cell line for NK cell studies due to its pronounced NK cell responsiveness. Our correlative and functional studies document that the role of B7-H6 applies to a broad spectrum of genotypically-diverse cell lines from many solid tumour types, the large majority of which have not been previously studied in terms of their NK cell sensitivity.

Our study's orthogonal use of PRISM and CRISPR identified previously underappreciated genes. Other biologically plausible genes which did not emerge prominently in our study should not necessarily be considered less important for regulation of NK cell cytotoxicity. For instance, some NK-activating ligands, such as ligands for NKG2D *(KLRK1)*, were not identified to be associated with higher responsiveness in the CRISPR screens, even though most of these proteins are expressed in the cell lines examined in our study[32-34]. One possible explanation is that loss-of-function screens for single genes may not detect as "hits" molecules that are functionally redundant because loss of one gene would be compensated by the unperturbed function of the other(s). Shedding of NKG2D ligands is another possible explanation, as their soluble form can block NK cell activation[35]. It is notable that *ex vivo*-expanded NK cells tend to gain NKG2A(*KLRC1*)/CD94(*KLRD1*), known to bind the inhibitory ligand HLA-E[16]. This may explain why *HLA-C* is not as prominent a "hit" in our CRISPR results as *HLA-E*. *Ex vivo* expansion of NK cells is currently (and potentially also for the foreseeable future) a key step in the application of NK cell immunotherapies, it is thus plausible that our study's observation for a key role of *HLA-E* may also reflect how NK cell-based therapies operate when administered *in vivo*. Interestingly, HLA-E was identified in only one of the two CRISPR screens performed on K562 cells co-cultured with NK cells[31], perhaps reflecting clonal differences in the specific cell line batches used in those studies, underscoring the value of performing CRISPR screens on more than one cell-line model.

Tumour cells with transcriptional signatures associated with NK cell sensitivity (including mesenchymal-like or chromatin remodeling signatures) are associated with ICI resistance in multiple clinical studies. These observations suggest that tumours highly enriched for mesenchymal molecular features; or tumours with primary or secondary resistance to ICI may represent attractive settings for future therapeutic applications of NK cell-based therapies, and that combined or sequential treatments of ICI and NK cell therapy may be beneficial to delay or overcome ICI resistance[5]. Therapeutic interventions reported to enhance tumour cell responses to cytotoxic T cells / ICI (including broad spectrum HDAC inhibitors[36]) may reverse the molecular signature of NK cell sensitivity in tumour cells and suppress their NK cell response,

raising cautionary note about potential combined use of these therapeutic modalities. HDAC inhibitors can also upregulate NKG2D ligands[37] and their effect on NK cell responses may thus vary from one cell type to another and be determined by the balance between treatment-induced changes in the inhibitory and activating signals.

Similar to other immune effector cell-based therapies, it is conceivable that anti-tumour activity of NK cells in patients will ultimately not depend only on the intrinsic cytotoxic potential of these cells or whether tumour cells' molecular features would be permissive to effective engagement and rapid lysis by the administered NK cells. Indeed, it is also important that NK cells infiltrate in high numbers the tumour sites and overcome local microenvironmental mechanisms that protect tumour cells from diverse pharmacological[38] or immune-based therapies[39]. Our current study focuses on *in vitro* co-cultures of tumour cells with donor-derived NK cells*,* as a basic model to define the landscape of cell-autonomous mechanisms that regulate tumour cell responsiveness to NK cells. The framework created by the current study can be applied in diverse other preclinical contexts, including use of other forms of NK cell-based therapies and/or preclinical models where tumour cells reside in the supportive local microenvironment of primary or metastatic lesions. Optimizing the potency, *in vivo* persistence, and tumour homing of NK cells or their ability to overcome stroma-induced protection of tumour cells[39], as well as understanding how NK cells may be influenced by their interaction with different types of tumour cells, are areas of active investigation: as the field builds consensus on how to address these considerations, the knowledge provided by this study will be an important resource and the basis for comprehensive approaches to use, both cell-autonomous and nonautonomous markers, to estimate the probability of anti-tumour responses of NK cells. Ultimately, the molecular signatures of NK cell response vs. resistance identified in our study and similar ones from future preclinical research can be examined in prospective samples from clinical studies and provide insights into which patients may be more likely to benefit (or not) from each one of the diverse types of NK cell-based therapies that are available in different stages of preclinical or clinical investigation.

Clinical studies of NK cell-based therapies have been already providing promising clinical outcomes (for example, chimeric antigen receptor-NK cells have clinical activity against relapsed or refractory CD19-positive hematologic malignancies[1]) which could further improve through biomarker-driven "personalized" administration of these therapies to patients whose tumours exhibit molecular features associated with NK cell sensitivity. Towards this goal, we

integrated PRISM and CRISPR studies to define the landscape of molecular features associated with NK cell sensitivity or resistance. Our results provide insights in our understanding of the NK-tumour cell interaction and may help inform current and future efforts to apply NK cell-based therapies for the treatment of human tumours.

Acknowledgements

This work was supported by the Stand Up To Cancer (SU2C) Convergence 2.0 Grant (M.S., A.C.C., C.S.M.), a collaboration by SU2C and the Society for Immunotherapy of Cancer; the SU2C Phillip A. Sharp Award for Innovation in Collaboration (Grant Number: SU2C-AACR-PS-22) (M.S., C.S.M.); the Claudia Adams Barr Program in Innovative Basic Cancer Research at Dana-Farber Cancer Institute (M.S., E.D., C.S.M., E.L.), the Human Frontier Science Program (HFSP) Fellowship (LT000834/2014-L, M.S.); the Leukemia and Lymphoma Society (LLS) Scholar Award (C.S.M.); and the Ludwig Center at Harvard (C.S.M.). The collaborating laboratories have also been partially supported by grants NIH R01 CA050947 (C.S.M.), CA196664 (C.S.M.), and U01 CA225730 (C.S.M.), de Gunzburg Myeloma Research Fund (C.S.M.); International Myeloma Society (C.S.M.), the Shawna Ashlee Corman Investigatorship in Multiple Myeloma Research (C.S.M.), Cobb Family Myeloma Research Fund (C.S.M.), the Department of Defense grants W81XWH-15-1-0012 (C.S.M.) and W81XWH-15-1-0013 (A.C.), the Finnish Cancer Organizations, Sigrid Juselius Foundation, Academy of Finland (S.M.), the Health Foundation Limburg, Nijbakker-Morra Stichting (N.B.) and the Dutch Cancer Association (KWF *Kanker Bestrijding*, UM2012-5375) (L.Wi.). The authors would like to thank Moshe Sade-Feldman for technical advice and discussion, Asaf Rotem for the gift of Malme-3M cell-line and Yosef Maruvka for assistance with MSI profiling.

Author contributions

M.S. and C.S.M conceived and designed the study overall.

M.S., E.L., N.B., S.N.A.A, M.B., C.C.M, J.A.R., O.Da., R.d.M.S., E.D., C.Y, Y.H., S.G., T.G., C.Z., L.Wa, L.Wi. C.S.M. contributed to design of individual experiments.

C.C.M., J.A.R., C.Y., T.G. provided critical reagents.

M.S., E.L., N.B., S.N.A.A, M.B., O.Da., S.B., C.Z., L.Wa., performed experiments

M.S., E.L., N.B., J.G.B., S.S.F., A.T., R.d.M.S., A.C.C., performed data analyses

M.S., J.A.R., A.T., J.G.B., O.Du. M.G., I.T., G.M.K., V.S., E.F., T.G., R.R., S.M., A.C.C., L.Wi., C.S.M. contributed to data interpretation.

M.S. and C.S.M. wrote the manuscript with input from all co-authors

Competing interests Statement

C.C.M., J.A.R., C.Y., T.G., L.Wi, M.S. and C.S.M. are authors of a patent application related to anti-tumour activity of NK cells. C.S.M. also discloses consultant/honoraria from Fate Therapeutics, Ionis Pharmaceuticals and FIMECS; employment of a relative with Takeda; and research funding from Janssen/Johnson & Johnson, TEVA, EMD Serono, Abbvie, Arch Oncology, Karyopharm, Sanofi, Nurix and H3 Biomedicine. M.G. receives research funding from Bristol-Myers Squibb and Merck. A.T. is a consultant for Tango Therapeutics. S.M. has received honoraria and research funding from Novartis, Pfizer and Bristol-Myers Squibb (not related to this study). The remaining authors declare no competing interests.

References

1 Liu, E. *et al.* Use of CAR-Transduced Natural Killer Cells in CD19-Positive Lymphoid Tumors. *N Engl J Med* **382**, 545-553, doi:10.1056/NEJMoa1910607 (2020).

2 Guillerey, C., Huntington, N. D. & Smyth, M. J. Targeting natural killer cells in cancer immunotherapy. *Nat Immunol* **17**, 1025-1036, doi:10.1038/ni.3518 (2016).

3 Nayyar, G., Chu, Y. & Cairo, M. S. Overcoming Resistance to Natural Killer Cell Based Immunotherapies for Solid Tumors. *Front Oncol* **9**, 51, doi:10.3389/fonc.2019.00051 (2019).

4 Shimasaki, N., Jain, A. & Campana, D. NK cells for cancer immunotherapy. *Nat Rev Drug Discov*, doi:10.1038/s41573-019-0052-1 (2020).

5 Gurjao, C. *et al.* Intrinsic Resistance to Immune Checkpoint Blockade in a Mismatch Repair-Deficient Colorectal Cancer. *Cancer Immunol Res* **7**, 1230-1236, doi:10.1158/2326-6066.CIR-18-0683 (2019).

6 Sade-Feldman, M. *et al.* Resistance to checkpoint blockade therapy through inactivation of antigen presentation. *Nat Commun* **8**, 1136, doi:10.1038/s41467-017-01062-w (2017).

7 Yu, C. *et al.* High-throughput identification of genotype-specific cancer vulnerabilities in mixtures of barcoded tumor cell lines. *Nat Biotechnol* **34**, 419-423, doi:10.1038/nbt.3460 (2016).

8 Doench, J. G. *et al.* Optimized sgRNA design to maximize activity and minimize off-target effects of CRISPR-Cas9. *Nat Biotechnol* **34**, 184-191, doi:10.1038/nbt.3437 (2016).

9 Sanjana, N. E., Shalem, O. & Zhang, F. Improved vectors and genome-wide libraries for CRISPR screening. *Nat Methods* **11**, 783-784, doi:10.1038/nmeth.3047 (2014).

10 Shalem, O. *et al.* Genome-scale CRISPR-Cas9 knockout screening in human cells. *Science* **343**, 84-87, doi:10.1126/science.1247005 (2014).

11 Ghandi, M. *et al.* Next-generation characterization of the Cancer Cell Line Encyclopedia. *Nature* **569**, 503-508, doi:10.1038/s41586-019-1186-3 (2019).

12 Brandt, C. S. *et al.* The B7 family member B7-H6 is a tumor cell ligand for the activating natural killer cell receptor NKp30 in humans. *J Exp Med* **206**, 1495-1503, doi:10.1084/jem.20090681 (2009).

13 Kaifu, T., Escaliere, B., Gastinel, L. N., Vivier, E. & Baratin, M. B7-H6/NKp30 interaction: a mechanism of alerting NK cells against tumors. *Cell Mol Life Sci* **68**, 3531-3539, doi:10.1007/s00018-011-0802-7 (2011).

14 Braud, V. M. *et al.* HLA-E binds to natural killer cell receptors CD94/NKG2A, B and C. *Nature* **391**, 795-799, doi:10.1038/35869 (1998).

15 Andre, P. *et al.* Anti-NKG2A mAb Is a Checkpoint Inhibitor that Promotes Anti-tumor Immunity by Unleashing Both T and NK Cells. *Cell* **175**, 1731-1743 e1713, doi:10.1016/j.cell.2018.10.014 (2018).

16 Kamiya, T., Seow, S. V., Wong, D., Robinson, M. & Campana, D. Blocking expression of inhibitory receptor NKG2A overcomes tumor resistance to NK cells. *J Clin Invest* **129**, 2094-2106, doi:10.1172/JCI123955 (2019).

17 Zhou, F. Molecular mechanisms of IFN-gamma to up-regulate MHC class I antigen processing and presentation. *Int Rev Immunol* **28**, 239-260, doi:10.1080/08830180902978120 (2009).

18 Dendoncker, K. *et al.* The nature of the GRE influences the screening for GR-activity enhancing modulators. *PLoS One* **12**, e0181101, doi:10.1371/journal.pone.0181101 (2017).

19 Rafehi, H. *et al.* Vascular histone deacetylation by pharmacological HDAC inhibition. *Genome Res* **24**, 1271-1284, doi:10.1101/gr.168781.113 (2014).

20 Sanchez, G. J. *et al.* Genome-wide dose-dependent inhibition of histone deacetylases studies reveal their roles in enhancer remodeling and suppression of oncogenic super-enhancers. *Nucleic Acids Res* **46**, 1756-1776, doi:10.1093/nar/gkx1225 (2018).

21 Pech, M. F. *et al.* Systematic identification of cancer cell vulnerabilities to natural killer cell-mediated immune surveillance. *Elife* **8**, doi:10.7554/eLife.47362 (2019).

22 Tawbi, H. A. *et al.* Pembrolizumab in advanced soft-tissue sarcoma and bone sarcoma (SARC028): a multicentre, two-cohort, single-arm, open-label, phase 2 trial. *Lancet Oncol* **18**, 1493-1501, doi:10.1016/S1470-2045(17)30624-1 (2017).

23 Burgess, M. A. *et al.* Clinical activity of pembrolizumab (P) in undifferentiated pleomorphic sarcoma (UPS) and dedifferentiated/pleomorphic liposarcoma (LPS): Final results of SARC028 expansion cohorts. *Journal of Clinical Oncology* **37**, 11015-11015, doi:10.1200/JCO.2019.37.15_suppl.11015 (2019).

24 Hugo, W. *et al.* Genomic and Transcriptomic Features of Response to Anti-PD-1 Therapy in Metastatic Melanoma. *Cell* **165**, 35-44, doi:10.1016/j.cell.2016.02.065 (2016).

25 Jerby-Arnon, L. *et al.* A Cancer Cell Program Promotes T Cell Exclusion and Resistance to Checkpoint Blockade. *Cell* **175**, 984-997 e924, doi:10.1016/j.cell.2018.09.006 (2018).

26 Riaz, N. *et al.* Tumor and Microenvironment Evolution during Immunotherapy with Nivolumab. *Cell* **171**, 934-949 e916, doi:10.1016/j.cell.2017.09.028 (2017).

27 Tirosh, I. *et al.* Dissecting the multicellular ecosystem of metastatic melanoma by single-cell RNA-seq. *Science* **352**, 189-196, doi:10.1126/science.aad0501 (2016).

28 Van Allen, E. M. *et al.* Genomic correlates of response to CTLA-4 blockade in metastatic melanoma. *Science* **350**, 207-211, doi:10.1126/science.aad0095 (2015).

29 Schwartzkopff, S. *et al.* Tumor-associated E-cadherin mutations affect binding to the killer cell lectin-like receptor G1 in humans. *J Immunol* **179**, 1022-1029, doi:10.4049/jimmunol.179.2.1022 (2007).

30 Freeman, A. J. *et al.* Natural Killer Cells Suppress T Cell-Associated Tumor Immune Evasion. *Cell Rep* **28**, 2784-2794 e2785, doi:10.1016/j.celrep.2019.08.017 (2019).

31 Zhuang, X., Veltri, D. P. & Long, E. O. Genome-Wide CRISPR Screen Reveals Cancer Cell Resistance to NK Cells Induced by NK-Derived IFN-gamma. *Front Immunol* **10**, 2879, doi:10.3389/fimmu.2019.02879 (2019).

32 Leung, W. H. *et al.* Modulation of NKG2D ligand expression and metastasis in tumors by spironolactone via RXRgamma activation. *J Exp Med* **210**, 2675-2692, doi:10.1084/jem.20122292 (2013).

33 Mou, X. *et al.* The regulatory effect of UL-16 binding protein-3 expression on the cytotoxicity of NK cells in cancer patients. *Sci Rep* **4**, 6138, doi:10.1038/srep06138 (2014).

34 Xu, X., Rao, G. & Li, Y. Xanthine oxidoreductase is required for genotoxic stress-induced NKG2D ligand expression and gemcitabine-mediated antitumor activity. *Oncotarget* **7**, 59220-59235, doi:10.18632/oncotarget.11042 (2016).

35 Ferrari de Andrade, L. *et al.* Antibody-mediated inhibition of MICA and MICB shedding promotes NK cell-driven tumor immunity. *Science* **359**, 1537-1542, doi:10.1126/science.aao0505 (2018).

36 Woods, D. M. *et al.* HDAC Inhibition Upregulates PD-1 Ligands in Melanoma and Augments Immunotherapy with PD-1 Blockade. *Cancer Immunol Res* **3**, 1375-1385, doi:10.1158/2326-6066.CIR-15-0077-T (2015).

37 Zhu, S. *et al.* The narrow-spectrum HDAC inhibitor entinostat enhances NKG2D expression without NK cell toxicity, leading to enhanced recognition of cancer cells. *Pharm Res* **32**, 779-792, doi:10.1007/s11095-013-1231-0 (2015).

38 McMillin, D. W. *et al.* Tumor cell-specific bioluminescence platform to identify stroma-induced changes to anticancer drug activity. *Nat Med* **16**, 483-489, doi:10.1038/nm.2112 (2010).

39 McMillin, D. W. *et al.* Compartment-Specific Bioluminescence Imaging platform for the high-throughput evaluation of antitumor immune function. *Blood* **119**, e131-138, doi:10.1182/blood-2011-04-348490 (2012).

Figures Legends

Fig. 1. Overview of the PRISM study using NK cells.

a, Schematic depiction of PRISM study.

b, AUC values calculated for each time point per cell line.

c, CTG cytotoxicity assays (see Methods) for individual cell lines. Data represent mean ± s.d.(5 replicates per line; two distinct experiments per line). P-values were calculated between the replicates of resistant vs. sensitive lines (two-way Mann-Whitney test, n=40 per group) in each E:T ratio.

Fig. 2. Overview of the genome-scale CRISPR studies of NK cell treatment.

a, Schematic depiction of CRISPR screens.

b, Histogram of gene-level $\log_2$-fold-changes (expressed as z-scores). Listed are examples of genes with prominent quantitative metrics (MAGECK rank analysis) across more than one screen.

Fig. 3. Mesenchymal-like tumour cells are on average more sensitive to NK cell cytotoxicity *in vitro*.

a, PCA of PRISM lines based on reverse phase protein array (RPPA) and on RNAseq data for 1000 most variable genes.

b, AUC (24hr) values for mesenchymal-like (n=292) vs. epithelial-like (n=235) cell lines (Box plots demarcate the first and third quartiles of the distribution; the median is shown in the center; and whiskers cover data within 1.5× the interquartile range of the box). two-sided Mann-Whitney tests.

c, Normalized expression levels (z-scores) for top 100 most differentially expressed (50 upregulated and 50 downregulated) genes in epithelial-like vs. mesenchymal-like cell lines.

d, Volcano plot for differential gene expression between epithelial-like and mesenchymal-like cell lines (adjusted p-values).

e, Left: AUC (24hr) distribution per tumour type, sorted by median AUC (Box plots plotted as described in **b**). Right: Percentage of epithelial-like and mesenchymal-like cell lines in each tumour type.

f, Left: Flow cytometry for staining with antibodies against CDH1 and VIM of two clones from an ovarian patient-derived tumour (n=1). Right: NK cytotoxicity assays (see Methods) of the two clones (n=3 distinct experiments with different NK cell donors).

Fig. 4. Key regulators of tumour cell responses to NK cells in PRISM and CRISPR studies

a, Scatter plot of quantitative metrics of significance for sgRNA enrichment or depletion (upper or lower panels, respectively) of each gene in CRISPR (y-axis) and for correlation of transcript expression with AUC in PRISM (24hr; x-axis). Highlighted genes are included in panel **b**.

b, Genes with significant differential expression (log_2 fold-changes) between NK cell-sensitive vs. resistant lines in PRISM (24hr) (left) and with significant sgRNA depletion or enrichment (z-scores of log_2 fold-changes) in ≥2 CRISPR screens and *RBBP4* in one screen (see Methods).

c, Flow cytometry of SW620 cells with sgRNA against *B7-H6* (*sgB7-H6*) or *OR10A2* as control (*sgCtrl*) stained with B7-H6 antibody. Unlabeled cells are colored grey, representative of n=2.

d, NK cytotoxicity assays (CTG) for colorectal cell lines with *sgB7-H6* or *sgCtrl* at E:T 2:1 (n=6 replicates per experiment, 3 distinct experiments per cell line; mean ± s.d.; SW620 $p=3.65x10^{-5}$, HCT15 $p=6.27x10^{-5}$, HT29 $p=3.23x10^{-7}$, Mann-Whitney two-sided tests, n=18).

e, Flow cytometry for live HT29 cells stained for B7-H6, after treatment with NK cells. Unlabeled control cells are colored grey. Lower panel: percentages of B7-H6 positive, B7-H6 negative cells (representative of n=2 experiments).

f, Schematic depiction of studies on role of B7-H6 on NK cell responses *in vivo*.

g, Tumor volume (caliper measurements; week 4) for NK cell-treated vs control tumors of SW620 cells with sgRNA for *sgB7-H6* or *sgCtrl* (two-sided Mann-Whitney tests, n=10 per group, median ± 95% CI).

h, Bioluminescence imaging (week 2) of mice receiving control (Left, "NK-") or NK treatment (Right, "NK+") (Color-coded scale on the right-hand side was used for images denoted by *).

Fig. 5. HLA-E as a major regulator of tumour cell responses to NK cells

a, Statistical significance of sgRNA depletion of HLA class I genes in genome-scale CRISPR knockout studies of NK cell-treated vs. control cells.

b, Flow cytometric staining for HLA-E, HLA-A/B/C in HT29 and SW620 cells with *sgSTAT1* or control sgRNA (*sgCtrl*) +/- IFNγ, representative of n=2 distinct experiments (grey: unlabeled control *sgCtrl* cells without treatment).

c-d, CTG cytotoxicity assays for HT29, SW620 cells with sgRNA against *STAT1* (*sgSTAT1*, **c**) or *HLA-E* (*sgHLA-E*, **d**) or common control knockouts (*sgCtrl*, sgRNA against *OR10A2*) at E:T 1:1 (5 different experiments per line using NK cells from 2-3 donors, n=6 replicates per experiment. (STAT1 $p=7.24x10^{-6}$, HLA-E $p=2.27x10^{-7}$, Mann-Whitney two-sided tests, n=30). Data (NK cell-induced cytotoxicity relative to respective NK cell-free control) are presented as mean ± s.d..

Fig. 6. Surface protein levels reveal functional relationship of B7-H6 and MHC class I molecules

a, Schematic representation for evaluation of surface protein levels using FACS-based sorting of PRISM pools of barcoded cell lines.

b, Left: Contour plot for B7-H6 surface levels (y-axis) vs side-scatter (x-axis), representative of n=4 FACS runs. Upper: Normalized read counts of each bin sorted by SPIN[40]. Middle: calculated protein scores. Lower: RNA expression levels of *B7-H6* in the corresponding cell lines ($R=0.47$, $p=5.21x10^{-22}$, Pearson correlation between surface protein scores and transcript levels).

c, same experimental setup as in **b,** with staining for anti-HLA-A/B/C antibody. Transcript levels or *B2M* and select HLA class I genes were compared with HLA-A/B/C protein scores ($R=0.44$, $p=8.48 \times 10^{-20}$, Pearson correlation between protein and *B2M* transcript levels).

d, Upper left: B7-H6 protein scores vs. AUC; χ^2 test, df=1. Results are shown for 24hr-AUC and are representative of results for the other time points. Upper right: Same setup, with staining for HLA-A/B/C protein scores. Lower left: scatter plot for surface protein scores of B7-H6 and HLA-A/B/C. Lower right quadrant represents the group of lines with both low surface HLA-A/B/C and high B7-H6 protein scores. Lower right: Venn diagram for intersection between cell line groups with low HLA-A/B/C and high B7-H6 (hypergeometric test).

Fig. 7. Transcriptional signatures associated with tumour cell responses to NK cells.

a, Normalized expression levels of genes from select pathways correlating with AUC in PRISM analyses (see Methods).

b, Correlation coefficients of transcript levels with *HLA-E* in TCGA datasets and in CCLE.

c, Log_2 fold changes of gene expression in cell lines treated with different HDAC inhibitors vs. respective controls[18-20].

d, sgRNA enrichment or depletion (log_2 fold changes) in K562 cells with high vs. low surface expression of MHC class I after IFNγ treatment[21].

e, Log_2 fold changes of transcript levels in non-responders vs. responders to ICI in melanoma[24-28] (see Methods). Baseline=pre-treatment.

f, Log_2 fold changes of transcript levels in LMS vs. UPS in TCGA data from sarcoma patients.

Fig. 8. GSEA for NK sensitivity and NK resistance gene sets in patient tumor samples

a, GSEA normalized enrichment scores (NES) for NK sensitivity or resistance gene sets (identified based on both CRISPR [MaGECK] and PRISM [Supplementary Table 5]) in melanoma tumors of non-responders vs. responders to ICI. Lack of significant changes ($p>0.05$) were colored white.

b, GSEA enrichment plots for non-responders vs. responders to ICI in the Riaz *et al.* dataset (included in panel **a**).

c, GSEA enrichment plots for LMS vs. UPS sarcoma tumours.

d, Schematic summary of landscape of molecular features associated with NK cell sensitivity vs. resistance

Methods

Cultures of tumor cells and primary NK cells

The PRISM pool of cell lines was cultured in RPMI 1640, in the absence of phenol red, with 10% heat-inactivated FBS and penicillin/streptomycin. Other cell lines were cultured in RPMI 1640 with 10% heat-inactivated FBS and penicillin/streptomycin. All cell lines were tested for mycoplasma using the MycoAlert kit. Cultures were incubated at 37°c with 5% CO_2. Details on the culture and experiments with ovarian cancer patient-derived samples are provided in Supplementary Note.

Primary NK cells were isolated from different anonymous healthy donors. For PRISM experiments, CD56+ NK cells were isolated using a NK cell negative selection kit (Miltenyi) and cultured in RPMI 1640 with 10% heat inactivated FBS, 10ng/ml IL-2 and penicillin/streptomycin. All other co-culture experiments were performed using expanded NK cell, isolated from healthy donors. To expand NK cells, CD3-depleted PBMCs (Stem Cell Kit, Lymphoprep) were cultured for 10-14 days in NK culture media (SCGM media with 10% heat-inactivated FBS, 10ng/ml IL-2, 1% Glutamax and penicillin/streptomycin) with a target density of $0.5x10^6$ cells/ml. The purity of the NK cells culture was determined by flow cytometry, using anti-CD56-APC (NCAM1, 1:100), anti-CD3-FITC (1:100). Cells were frozen in SCGM media with 7% DMSO and 20% heat inactivated FBS. Upon thawing, cells were cultured in the NK culture media, supplemented with 20% conditioned media collected at the time of expansion. NK cell profiling was determined by flow cytometry using antibodies against CD56 (NCAM1, 1:100), NKG2D (KLRK1, 1:100), NKp46 (NCR1, 1:10), NKp30 (NCR3, 1:40), NKG2A (KLRC1, 1:100), NKG2C (KLRC2, 1:100), KLRG1 (1:40). We observed similar qualitative patterns of expression for selected NK markers across donors and modest quantitative differences between some batches for individual markers (data not shown).

PRISM-based phenotypic studies in pooled format to quantify NK cell cytotoxicity against DNA-barcoded cancer cell lines

PRISM allows phenotypic screens with pools of different cancer cell lines each harboring a distinct DNA barcode as previously described[7]. Briefly, 568 adherent cancer cell lines, stably transduced with their respective DNA barcode sequences were seeded in 25 cm^2 flasks ($100x10^3$ cells/flask) in experimental replicates, 6 for controls without NK cells and 3 per effector-to-target (E:T) ratio and for each different time points (24, 48 and 72 hours). Cells were incubated in 5 ml PRISM growth media for 24 hours: at that point, primary NK cells were washed, resuspended in PRISM growth media and added to the PRISM cell cultures in 4-5 different E:T ratios of 10:1,5:1,2.5:1 and 1.25:1 (1 ml/flask; for 24hr we examined an additional E:T of 0.625:1). Control flasks were supplemented with the same volume of media only. At 24, 48 and 72 hours post-NK coculture, adherent cells of the respective flask were washed with PBS and incubated for 1 hour at 60ºC in lysis buffer (1 ml per flask), prepared using doubled distilled water with 10% PCR buffer (20mM Tris-HCL pH 8.4, 50mM KCL), 0.45% NP40, 0.45% TWEEN and 10% proteinase K. The DNA from the lysates, which contained the "DNA barcode" sequences for different cell lines of the PRISM panel, was amplified and sequenced as previously

described[7]. The log_2 ratios of read counts for the barcode of each cell line in the replicates of each E:T ratio vs. their respective controls (without NK cells) were used to calculate the area under the curve (AUC) of tumour cell survival, representing a quantitative measure of the resistance of each cell line to NK cell cytotoxicity. For all figures, 24hr-AUCs are shown as representative for the other time points.
In this study, the terms NK cell "sensitivity" / "sensitive" cells vs. "resistance" / "resistant" cells are used interchangeably with the terms "low AUC" vs. "high AUC", respectively, and refer to the relative ranking of cell lines of our PRISM panel according to their AUC, as a quantitative metric of their response to NK cells, rather than a binary status for NK cell killing of all vs. none of the cells of an individual cell line. We did not observe a specific cutoff point or major "gap" of AUC values which clearly separates all sensitive vs. all resistant lines. Instead, the large majority of cell lines are distributed along a quantitative continuum of responses between the highest and lower observed AUC levels. Most analyses correlating AUC values with molecular data took into account the whole range of AUCs. Some analyses involved dichotomization of the PRISM panel to groups of lines with "lower AUC" ("sensitive") vs. "higher AUC" ("resistant"), based on AUC cutoff points (e.g., lower vs. upper tertiles; or median AUC value), as indicated in the respective Figure Legends or other parts of this Methods section.

Correlation of molecular profiling data with AUC values from PRISM study

RNAseq, RPPA and mutation data on the cell lines of the PRISM panel were accessed through the molecular profiling data of these cell lines within the larger CCLE panel, which have been previously released by the Broad Institute of MIT and Harvard[11]. Further details on the analyses which examined the correlation of these molecular profiling data with the AUC values from the PRISM study of NK cell treatment are provided in Supplementary Note.

Genome-scale CRISPR gene editing screens

Genome-scale CRISPR gene editing screens to define determinants of tumor cell response vs. resistance to NK cells were performed using reagents and protocols similar to previous studies by other groups[8-10] or ours[41]. The cell lines chosen for these screens were HCT15 (*B2M* mutant and hypersensitive to NK cells); SW620 (highly NK cell-sensitive line with mesenchymal-like transcriptional signature); and HT29 (intermediately sensitive cell line with epithelial-like signature). The genome-scale sgRNA libraries GeCKO V2 (sub-libraries V2.1 and V2.2 for HCT15 cells) and *Brunello* (for SW620 and HT29 cells) were applied. Each cell line was examined with 3-4 distinct biological replicates, involving tumour cells treated with NK cells from different donors vs. their respective control. Each replicate was treated on consecutive days and involved co-culture for 6 hours with primary NK cells expanded from its respective donor. The selected E:T ratio of each line was selected to kill ~50% of the tumour cells. The number of tumour cells in each replicate had a target sgRNA representation of 500-1000 cells/sgRNA. After each screen, DNA extraction, PCR amplification and next generation sequencing, as

well as processing of sequencing results were performed similar to prior studies (e.g.[10] and[41]) to quantify the distribution of sgRNAs in the NK cell-treated vs. control samples in each screen. One-sided test for enrichment or depletion of the sgRNAs and sgRNA rank aggregation was performed for each gene using MaGECK (Model-based Analysis of Genome-wide CRISPR-Cas9 Knockout), with default parameter settings[42]. Olfactory receptor genes (generally not expressed or considered to influence tumour cell immune responses) were used to establish a control distribution of sgRNAs for the rank aggregation procedure. Based on MaGECK output, a gene was considered to exhibit a significant enrichment/depletion of its sgRNAs, if it satisfied the following conditions: p-value≤0.05, enriched (or depleted) sgRNA≥2, rank of enrichment or depletion ≤2000 and RPKM>1 (CCLE RNAseq dataset[11]) in the respective cell line. STARS, a negative binomial distribution method[8], was run as a complementary approach to assess enrichment or depletion of sgRNAs, using the average $\log_2$-fold change of normalized readcounts of sgRNAs for a given gene, across all replicates in each screen. Emphasis was placed on genes with significant enrichment/depletion of their sgRNAs concordantly for both MaGECK and STARS within a screen of a specific cell line, or across CRISPR screens in multiple cell lines; and also between CRISPR and PRISM results. None of these identified genes belonged to the olfactory receptor set.

Further details on genome-scale CRISPR screens and on experiments for CRISPR-based studies of individual genes are provided in Supplementary Note.

NK cell cytotoxicity assays

To examine if NK cell cytotoxicity results obtained in pooled format by PRISM are concordant to those obtained by conventional testing of individual cell lines in non-pooled format, 8 individual cell lines (from several different cancer types) without the “DNA barcode” were tested as examples of NK cell-sensitive vs. -resistant lines: Cell Titer Glow (CTG) viability assays were performed for each cell line in 6 different E:T ratios: controls (no NK, E:T 0:1), 0.3:1, 0.6:1, 1.25:1, 2.5:1 and 5:1, with 5 replicates per experimental condition. Every plate had a set of wells which were seeded only with NK cells. Tumour cells were seeded in 384 plates (5,000 cells per well in 50 µL growth media) and after overnight incubation, primary NK cells (cell suspension of 50 µL per well) were added for 6 hours. Similar approaches were applied in CTG assays for single-gene CRISPR knockouts of *B7-H6*, *STAT1*, *HLA-E* and (as control knockout) *OR10A2*, except the latter experiments were performed with n=6 replicates per experimental condition. Tumour cells were seeded in 384 plates (10,000 cells per well in 20µl growth media) and, after overnight incubation, NK cells from different donors (20 µL per well) were added in the cultures for 4 hours.

At the end of these assays, 10% CTG was added to each well for 20 minutes incubation and the plates were read with a microplate reader (BioTek Synergy 2, BioTek, Winooski, VA). In these CTG assays, NK cytotoxicity against each cell line was calculated for each E:T ratio as follows:

$$\text{Cytotoxicity(X)} = 1 - \frac{\text{X} - \text{average(NK only)}}{\text{average(controls)}}$$

Two-sided Mann-Whitney tests were applied to compare the NK cytotoxicity between NK- sensitive vs. -resistant lines of the PRISM study for each E:T ratio; or between CRISPR knockout of a given gene of interest vs. control knockout. The statistical significance of these comparisons was also confirmed with two-way analyses of variance and Sidak post-hoc tests.

NK cell cytotoxicity against tumor cells was also assessed by flow cytometry assays in different configurations. For these assays, tumour cells were typically plated at a concentration of $2x10^5$ cells/well in 6-well plates overnight, washed with fresh media and then treated with primary NK cells (that had been labeled with eFluor 450 per manufacturer's instruction) for 6 hours. Cells in suspension and (after their trypsinization) adherent cells were collected from each well, incubated for 30 min at 37^{o}C for recovery and then stained using the LIVE/DEAD Fixable Green Dead Cell Stain Kit (1:1000) for 30 min on ice, followed by 15 min incubation with 4% formalin on ice. Cytotoxicity was calculated as a ratio (1 – [percent of live cells in a given E:T ratio / percent of live tumor cells in control cultures without NK cells]) after gating on cells negative for both eFluor 450 and green fluorescence which represent the live tumour cell population.

For cocultures of NK cells (labeled with eFluor 450) with HT29 tumour cells (which exhibit heterogeneous expression of B7-H6) and the monitoring of B7-H6 surface expression on the residual live tumour cells (Fig. 4e), cells were stained with both LIVE/DEAD Fixable Green Dead Cell Stain (1:1000) and anti-B7-H6 antibody (APC conjugated, 1:10) for 30 min on ice and surface B7-H6 expression was assessed after gating on the live tumour cell population (negative for both eFluor 450 and green fluorescence).

For NK cell cocultures of the ovarian carcinoma clones which were expressing tdTomato (see Supplemental Information), cytotoxicity was assessed by LIVE/DEAD Fixable Green Dead Cell Stain after gating on the live tdTomato-labeled tumour cells. These cocultures were performed with NK cells derived from three different donors. In NK cell cytotoxicity assays against SW620 cells with vs. without pretreatment with panobinostat, tumor cells were separated in 2 groups and stained with either CFSE or eFluor 450 per manufacturer's instructions. Each of these differentially labeled tumor cell populations was plated in 6-well plates ($6x10^5$ cells/well) and were then treated for 12 hours with either DMSO or the broad spectrum HDAC inhibitor panobinostat (12.5nM). After washout, fresh drug-free media were added and *in vitro*-expanded primary donor-derived NK cells were added for 6 hours at different E:T ratios. Two washes with PBS, to remove NK cells and dead cells, and trypsinization for tumour cell detachment were performed. The DMSO- or panobinostat-pretreated tumour cell samples (which had been labeled with different fluorophores) and exposed to NK cells at the same E:T ratio were combined

and fixed with 4% formalin for 15 minutes on ice. Relative cytotoxicity for panobinostat- vs. DMSO-pretreated cells was assessed by flow cytometry and calculated for each E:T ratio vs. control cultures without NK cells as a ratio, i.e. (1 – [percent of CFSE-positive cells in a given E:T ratio / percent of CFSE-positive cells in control cultures without NK cells]) or conversely (1 – [percent of eFluor450-positive cells in a given E:T ratio / percent of eFluor450-positive cells in control cultures without NK cells). Flow cytometric analyses were performed on a BD LSRFortessa™ cell analyzer (BD Biosciences, Inc).

Mesenchymal-like transcriptional signature

Principal component analyses of proteomic and transcriptional profiles were used to identify two main lineage clusters of cell lines exhibiting epithelial-like vs. mesenchymal-like characteristics. A transcriptional score of mesenchymal-like state was calculated based on the average normalized expression of the top 50 genes that were over-expressed in the mesenchymal-like cluster compared with the epithelial-like cluster (Fig. 3c in manuscript). The terms “epithelial-like” vs. “mesenchymal-like” refer in this study to the constitutive state of the respective cell lines under conventional culture conditions, in the absence of any stimuli (e.g., cytokines, growth factors, genetic/epigenetic perturbations) that might cause epithelial-to-mesenchymal transition (EMT) or its reverse transition (MET). Additional future research is warranted to examine if either of these transitions (EMT or MET) can also be associated with significant changes in the extent of NK cell sensitivity of a genotypically diverse spectrum of cell lines.

***In vivo* experiments**

Female NOD.Cg-*Prkdc*^{scid} Il2rg^{tm1Wjl}/SzJ (NSG) mice (Jackson Laboratory) were housed and fed with autoclaved food and water at the Dana-Farber Cancer Institute (DFCI) Animal Research Facility (ARF). Animal studies were performed according to a protocol approved by the Dana-Farber Cancer Institute Animal Care and Use Committee, mice were maintained on a 12-h/12-h light/dark cycle under ambient temperature and humidity. Mice aged 6 weeks were divided into a control group and a NK cell-treated group. In this experiment, we applied the Winn assay[43-47], to co-inject subcutaneously tumour and NK cells, and test the effect of NK cells in the tumour microenvironment. Control mice (n=10) were injected subcutaneously with 2x10^6 SW620-*Cas9*-luc transfected with sgRNAs against *B7-H6* (*sgB7-H6*) to the right flank and with 2x10^6 SW620-Cas9-luc transfected with sg*OR10A2* (sgRNAs against *OR10A2*; olfactory receptor gene which is considered to have no impact on tumour cell response to immune effector cells) as control knockouts (*sgCtrl*) to the left flank. The NK cell-treated groups (n=10) were injected subcutaneously with a mix of 2x10^6 primary NK cells and 2x10^6 SW620-*Cas9*-luc transfected with sgRNAs against *B7-H6* to the right flank and with a mix of 2x10^6 primary NK cells and 2x10^6 SW620-*Cas9*-luc transfected with sgRNAs against *OR10A2* as control knockouts to the left flank. The

NK and tumours cells were mixed right before the injections. Bioluminescence measurements were taken weekly at the DFCI ARF. Two-way Mann-Whitney tests were applied between groups. Statistical significance of results for comparison of signal (log_{10}) was also confirmed with one-way analysis of variance (e.g. Brown-Forsyth Welch test and Dunnet's T3 post-hoc tests). Caliper measurements were taken at the end of the experiment before tumour collection (nonpalpable tumors were assigned tumor volume of 1 mm^3 for data visualization, Fig. 4g). Two-way Mann-Whitney test was applied for comparison of tumor burden between groups. Statistical significance of results was also confirmed with one-way analysis of variance (e.g. Brown-Forsyth Welch test and Dunnet's T3 post-hoc tests).

PRISM-based surface protein level evaluation

PRISM pools of cell lines were stained with antibody against HLA/A/B/C (Alexa-488 conjugated, 5µl/10^6 cells) or against B7-H6 (PE conjugated, 10µl/10^6 cells) on ice for 40 or 90 minutes, respectively (4 replicates per antibody; 10^7 cells/replicate). Each replicate was FACS-sorted based on negative, low, medium and high fluorescence levels using a BD FACSAria II Cell Sorter. For each antibody staining, 6 replicates of 10^6 cells each were kept as unsorted controls. Following lysis (as described above), DNA material (containing the "DNA barcodes" of each respective cell line) from each FACS-sorted or unsorted sample was amplified and sequenced as described above for PRISM assays to determine the read counts of each "DNA barcode" and its corresponding cell line in each sample. Data were normalized according to the median of total read counts across samples and were log_2 transformed. Cell lines with low representation in the unsorted controls were filtered out. Z-scores per cell line were calculated and results across samples were sorted by SPIN[40]. Surface protein scores were then calculated from the SPIN-sorted data using polynomial curve fitting (degree=3). In view of the dynamic range of the B7-H6 antibody staining, the upper two bins and the lower two bins were combined into 'high' and 'low' surface expression, respectively. Analysis was performed on all lines with available protein scores for both B7-H6 and HLA-A/B/C (n=383). Pearson correlation coefficients (and respective p-values) between surface protein scores and transcript levels for various genes were calculated using the two-sided Matlab *corr* function. Association of surface protein scores with AUC values was evaluated by χ^2 test.

Gene Set Enrichment Analysis (GSEA)

GSEA was performed using the pre-ranked option on the MSigDB collections KEGG, Biocarta, PID and additional three custom sets described at Supplementary Table 6. Further details are provided in Supplementary Note.

Statistics and reproducibility

For CRISPR screens, each replicate was performed as a separate experiment using different donor NK cells. For the cytotoxic assays, n refers to the number of replicates, and the number of distinct experiments is stated in the figure legends. For those NK cell cytotoxic assays with n≤4 replicates, p-values were not calculated. Statistical tests were performed using two-sided Mann-Whitney test, unless stated otherwise. P-values for CRISPR were calculated by MAGECK, p-values for correlation were calculated by *Matlab corr* function. Adjusted *P* values (*q*-values) were calculated in the case of multiple testing using the Benjamini–Hochberg adjustment.

Software

Matlab R2013b	https://www.mathworks.com/products/matlab.html
MaGECK 0.5.2	https://sourceforge.net/projects/mageck/
GSEA 2-2.2.3 pre-ranked	http://software.broadinstitute.org/gsea/index.jsp
PRISM 8 Graphpad	https://www.graphpad.com/scientific-software/prism/
R 3.5.3	https://rstudio.com/
FlowJo 10	https://www.flowjo.com/
cutadapt v1.9.1	http://journal.embnet.org/index.php/embnetjournal/article/view/200
firehose_get	https://gdac.broadinstitute.org/
STARS 1.0@134828e	https://portals.broadinstitute.org/gpp/public/analysis-tools/crispr-gene-scoring
BioRender	https://BioRender.com
BD FASCDiva 8.0.1,	https://www.bdbiosciences.com/en-us/instruments/research-instruments/research-software/flow-cytometry-acquisition/facsdiva-software

Data Availability Statement

TCGA data were acquired from the Broad Firehose web site, version 2016_07_15. Readcounts from the CRISPR and PRISM screens are available in Supplemental Table 4. Raw data can be available upon request. Molecular profiling data of tumor cells treated with broad spectrum HDAC inhibitors were accessed from Gene Expression Omnibus (GEO; GSE108191, GSE96649, GSE101708 and GSE37376). RNAseq data of tumors from patients treated with ICI were accessed from GEO: GSE115978 (Jerby-Arnon et al.[25]), GSE91061 (Riaz et al.[26]), GSE78220 (Hugo et al.[24]). The Van-Allen dataset was acquired from dbGaP (accession phs000452.v2.p1[28]).

Code Availability Statement

The study did not develop new software of custom code, but applied in sequence different previously available codes for which details are provided in the Online Methods and Supplemental Information. All code used in this study can be available upon request.

Methods-only References

40 Tsafrir, D. *et al.* Sorting points into neighborhoods (SPIN): data analysis and visualization by ordering distance matrices. *Bioinformatics* **21**, 2301-2308, doi:10.1093/bioinformatics/bti329 (2005).

41 Shirasaki, R. *et al.* Functional Genomics Identify Distinct and Overlapping Genes Mediating Resistance to Different Classes of Heterobifunctional Degraders of Oncoproteins. *Cell Rep* **34**, 108532, doi:10.1016/j.celrep.2020.108532 (2021).

42 Li, W. *et al.* MAGeCK enables robust identification of essential genes from genome-scale CRISPR/Cas9 knockout screens. *Genome Biol* **15**, 554, doi:10.1186/s13059-014-0554-4 (2014).

43 Lozupone, F. *et al.* Effect of human natural killer and gammadelta T cells on the growth of human autologous melanoma xenografts in SCID mice. *Cancer Res* **64**, 378-385, doi:10.1158/0008-5472.can-03-1501 (2004).

44 Bobisse, S. *et al.* Reprogramming T lymphocytes for melanoma adoptive immunotherapy by T-cell receptor gene transfer with lentiviral vectors. *Cancer Res* **69**, 9385-9394, doi:10.1158/0008-5472.CAN-09-0494 (2009).

45 Eisenberg, V. *et al.* Targeting Multiple Tumors Using T-Cells Engineered to Express a Natural Cytotoxicity Receptor 2-Based Chimeric Receptor. *Front Immunol* **8**, 1212, doi:10.3389/fimmu.2017.01212 (2017).

46 Gunnarsdottir, F. B., Kiessling, R. & Pico de Coana, Y. Establishment of Melanoma Tumor Xenograft Using Single Cell Line Suspension and Co-injection of Patient-Derived T Cells in Immune-Deficient NSG Mice. *Methods Mol Biol* **1913**, 207-215, doi:10.1007/978-1-4939-8979-9_15 (2019).

47 Jakka, G. *et al.* Antigen-specific in vitro expansion of functional redirected NY-ESO-1-specific human CD8+ T-cells in a cell-free system. *Anticancer Res* **33**, 4189-4201 (2013).

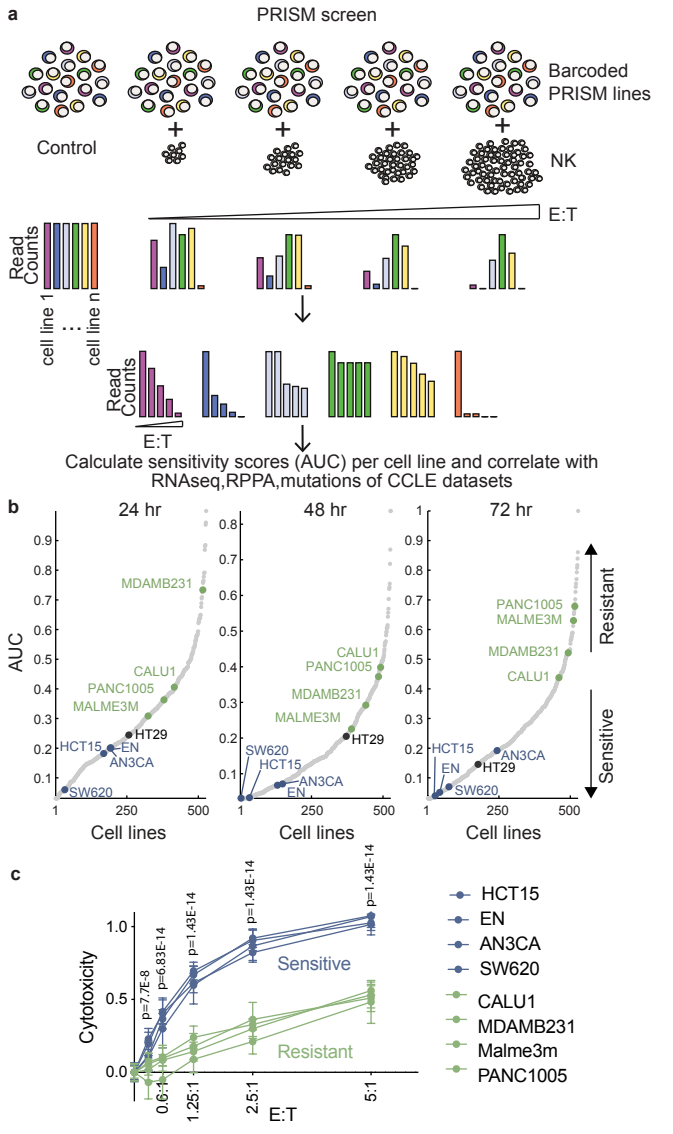
a
PRISM screen
Barcoded
PRISM lines
Control
NK
E:T
Read
Counts
cell line 1
cell line n
Read
Counts
E:T
Calculate sensitivity scores (AUC) per cell line and correlate with
RNAseq,RPPA,mutations of CCLE datasets
b
24 hr
48 hr
72 hr
AUC
Cell lines
MDAMB231
CALU1
PANC1005
MALME3M
HT29
HCT15
EN
AN3CA
SW620
Resistant
Sensitive
c
Cytotoxicity
E:T
0.6:1
1.25:1
2.5:1
5:1
p=7.7E-8
p=6.83E-14
p=1.43E-14
p=1.43E-14
p=1.43E-14
Sensitive
Resistant
HCT15
EN
AN3CA
SW620
CALU1
MDAMB231
Malme3m
PANC1005

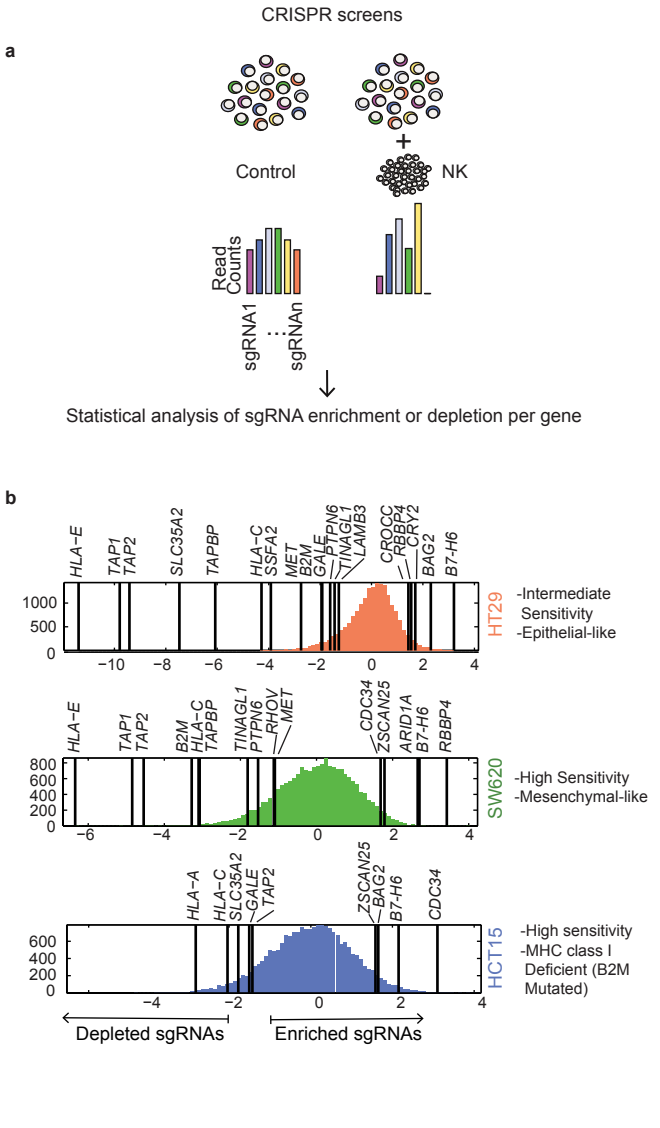
CRISPR screens
a
Control
NK
Read Counts
sgRNA1
sgRNAn
Statistical analysis of sgRNA enrichment or depletion per gene
b
HLA-E
TAP1
TAP2
SLC35A2
TAPBP
HLA-C
SSFA2
MET
B2M
GALE
PTPN6
TINAGL1
LAIMB3
CROCC
RBBP4
CXR2
BAG2
B7-H6
HT29
-Intermediate Sensitivity
-Epithelial-like
SW620
-High Sensitivity
-Mesenchymal-like
HCT15
-High sensitivity
-MHC class I Deficient (B2M Mutated)
Depleted sgRNAs
Enriched sgRNAs

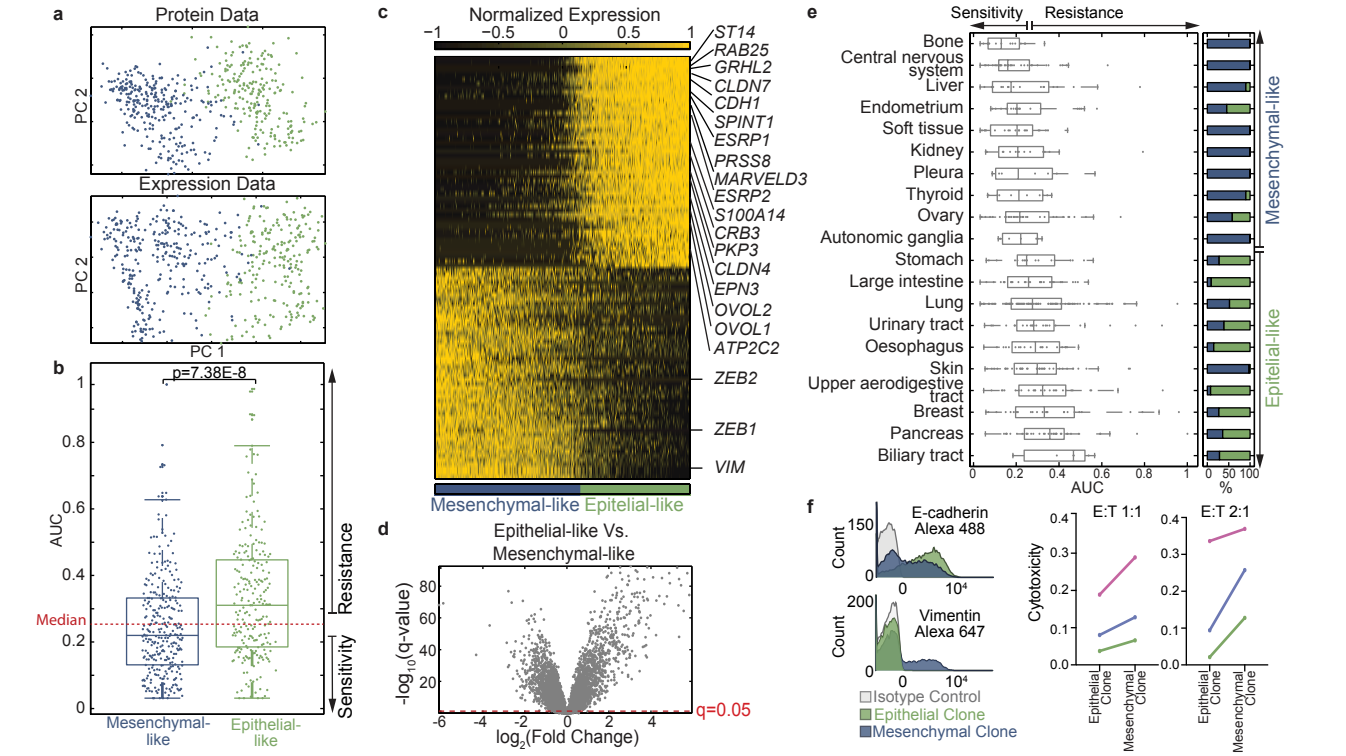
a
Protein Data
PC 2
Expression Data
PC 2
PC 1
b
p=7.38E-8
AUC
Median
Mesenchymal-like
Epithelial-like
Resistance
Sensitivity
c
Normalized Expression
−1
−0.5
0
0.5
1
ST14
RAB25
GRHL2
CLDN7
CDH1
SPINT1
ESRP1
PRSS8
MARVELD3
ESRP2
S100A14
CRB3
PKP3
CLDN4
EPN3
OVOL2
OVOL1
ATP2C2
ZEB2
ZEB1
VIM
Mesenchymal-like
Epitelial-like
d
Epithelial-like Vs.
Mesenchymal-like
-log10(q-value)
log2(Fold Change)
q=0.05
e
Sensitivity
Resistance
Bone
Central nervous system
Liver
Endometrium
Soft tissue
Kidney
Pleura
Thyroid
Ovary
Autonomic ganglia
Stomach
Large intestine
Lung
Urinary tract
Oesophagus
Skin
Upper aerodigestive tract
Breast
Pancreas
Biliary tract
AUC
%
Mesenchymal-like
Epitelial-like
f
E-cadherin
Alexa 488
Vimentin
Alexa 647
Count
Isotype Control
Epithelial Clone
Mesenchymal Clone
E:T 1:1
E:T 2:1
Cytotoxicity
Epithelial Clone
Mesenchymal Clone

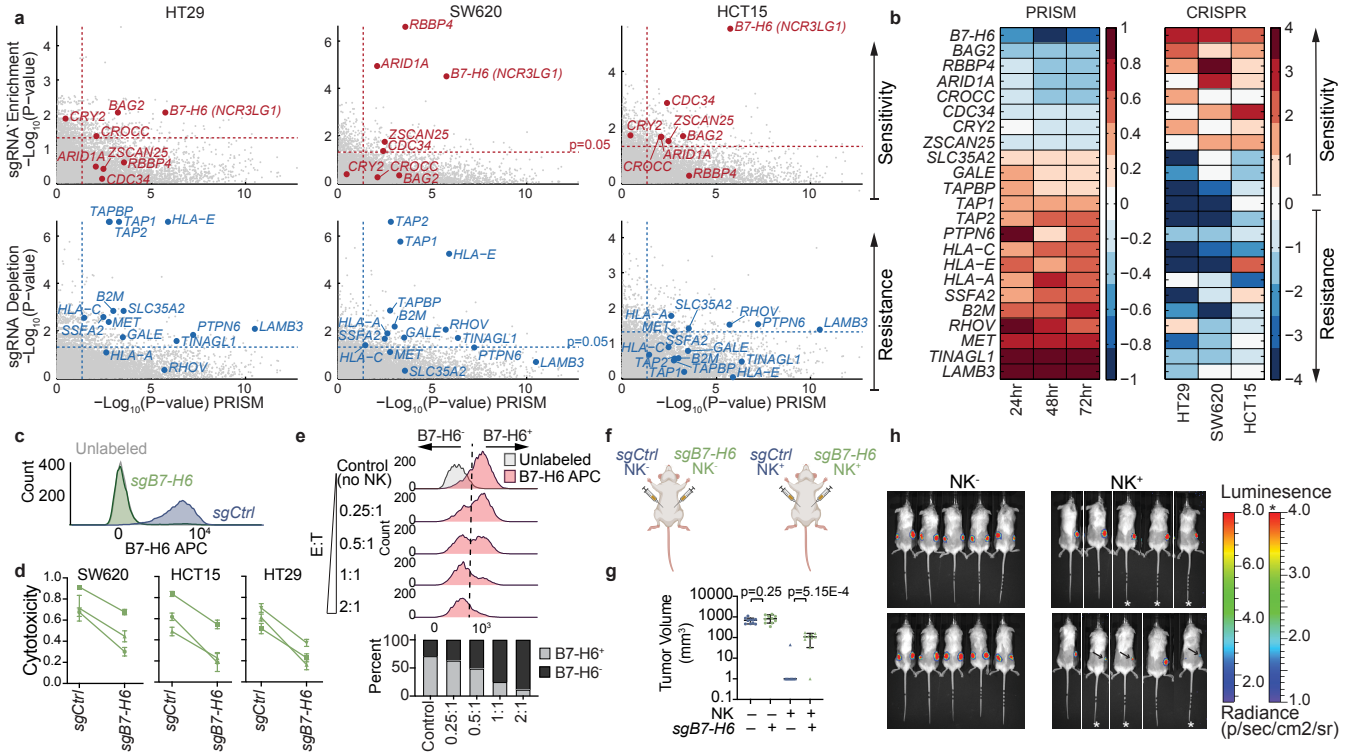
a
HT29
SW620
HCT15
sgRNA Enrichment −Log10(P−value)
sgRNA Depletion −Log10(P−value)
−Log10(P−value) PRISM
Sensitivity
Resistance
p=0.05
p=0.05
RBBP4
ARID1A
B7-H6 (NCR3LG1)
CDC34
CRY2
BAG2
ZSCAN25
CROCC
TAPBP
TAP1
TAP2
HLA−E
B2M
HLA−C
SLC35A2
MET
SSFA2
GALE
PTPN6
LAMB3
TINAGL1
HLA−A
RHOV
b
PRISM
CRISPR
B7-H6
BAG2
RBBP4
ARID1A
CROCC
CDC34
CRY2
ZSCAN25
SLC35A2
GALE
TAPBP
TAP1
TAP2
PTPN6
HLA−C
HLA−E
HLA−A
SSFA2
B2M
RHOV
MET
TINAGL1
LAMB3
24hr
48hr
72hr
HT29
SW620
HCT15
Sensitivity
Resistance
c
Unlabeled
sgB7-H6
sgCtrl
Count
B7-H6 APC
d
SW620
HCT15
HT29
Cytotoxicity
sgCtrl
sgB7-H6
e
B7-H6−
B7-H6+
Control (no NK)
0.25:1
0.5:1
1:1
2:1
E:T
Unlabeled
B7-H6 APC
Count
Percent
B7-H6+
B7-H6−
Control
f
sgCtrl
sgB7-H6
NK−
NK+
g
Tumor Volume (mm3)
p=0.25
p=5.15E-4
NK
sgB7-H6
h
NK−
NK+
Luminescence
Radiance (p/sec/cm2/sr)

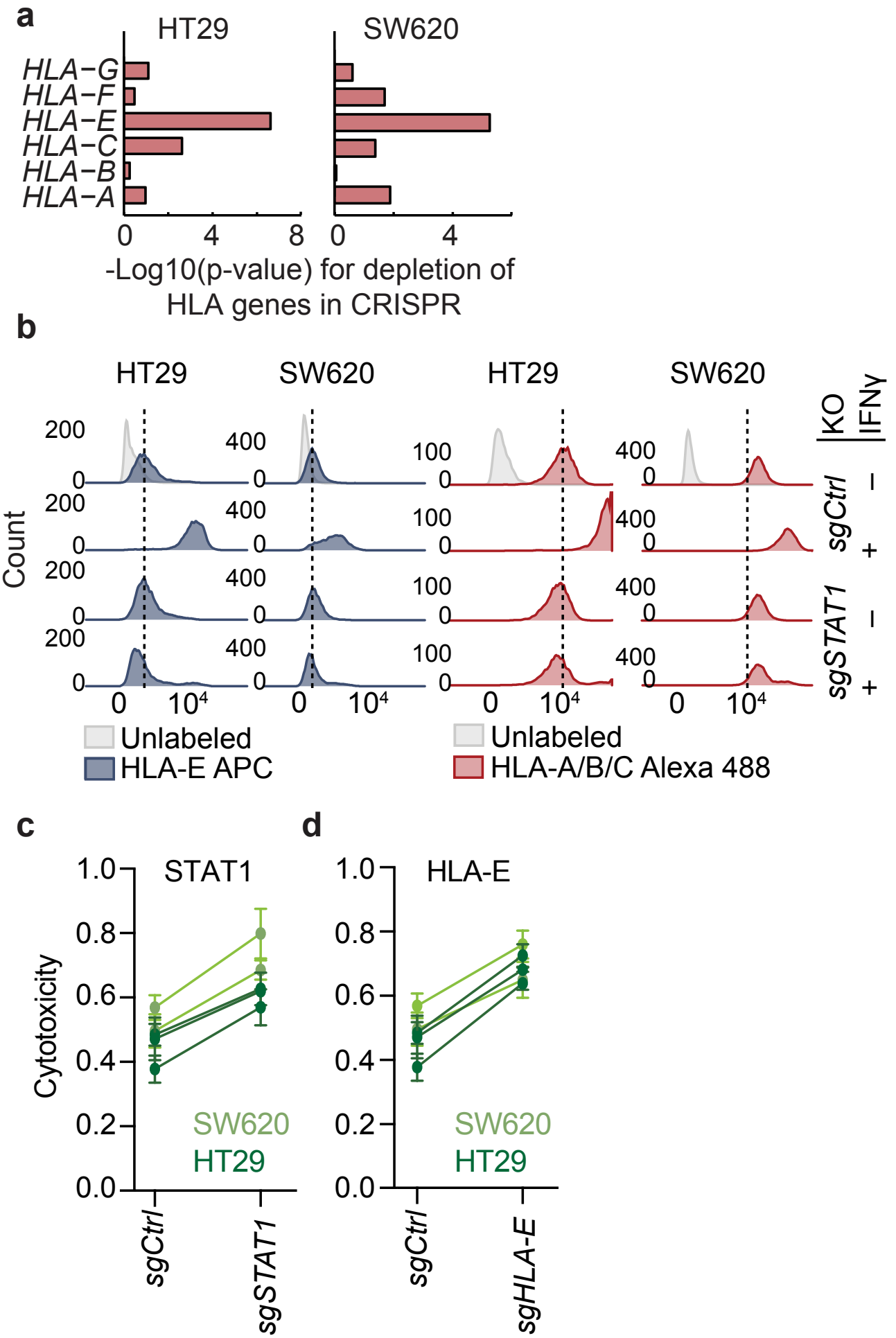
a
HT29
SW620
HLA-G
HLA-F
HLA-E
HLA-C
HLA-B
HLA-A
0
4
8
0
4
-Log10(p-value) for depletion of HLA genes in CRISPR
b
HT29
SW620
HT29
SW620
KO
IFNγ
sgCtrl
sgSTAT1
Count
200
400
100
10^4
Unlabeled
HLA-E APC
Unlabeled
HLA-A/B/C Alexa 488
c
STAT1
Cytotoxicity
1.0
0.8
0.6
0.4
0.2
0.0
SW620
HT29
sgCtrl
sgSTAT1
d
HLA-E
sgCtrl
sgHLA-E

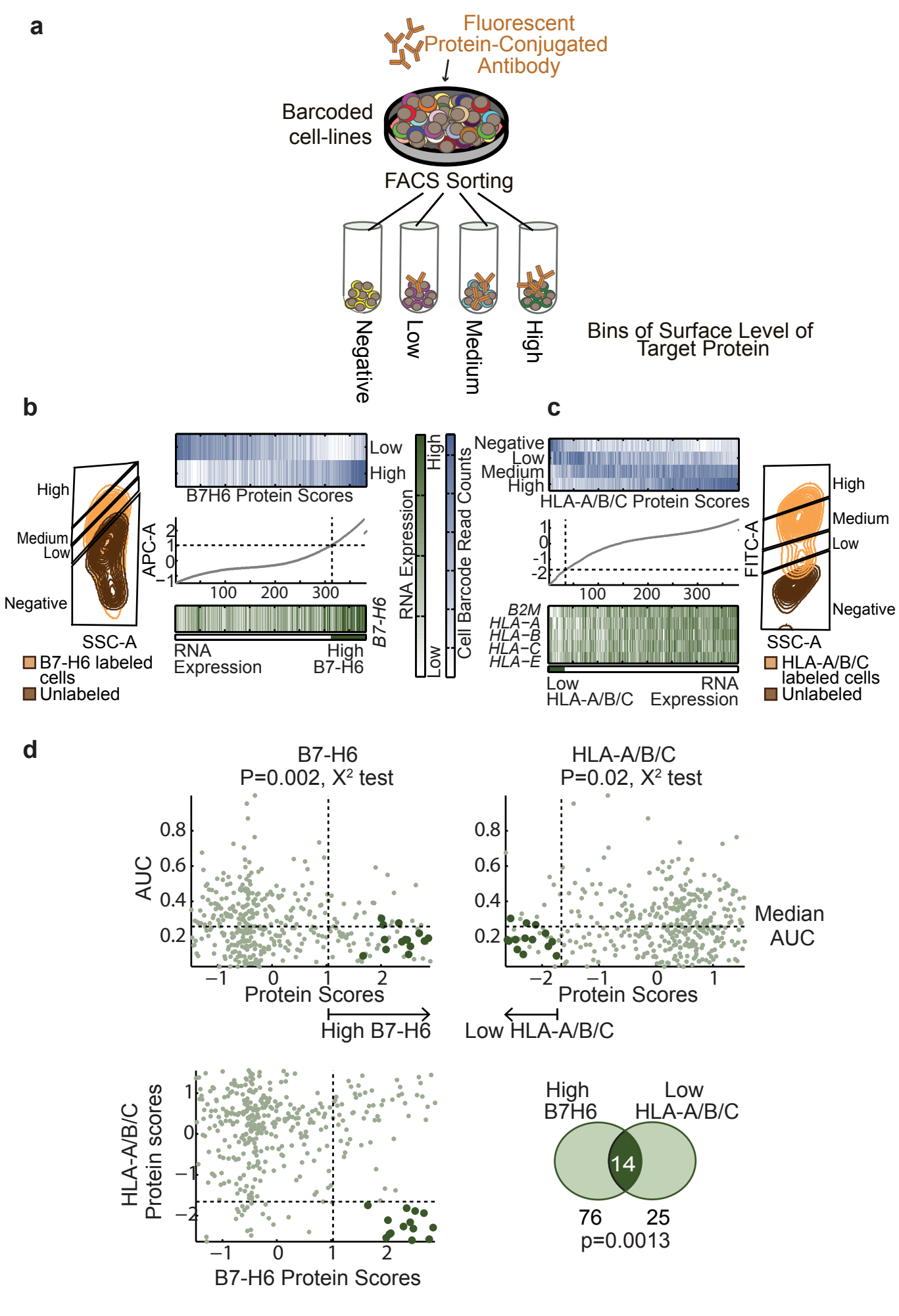
a
Fluorescent Protein-Conjugated Antibody
Barcoded cell-lines
FACS Sorting
Negative
Low
Medium
High
Bins of Surface Level of Target Protein
b
High
Medium
Low
Negative
SSC-A
B7-H6 labeled cells
Unlabeled
APC-A
B7H6 Protein Scores
Low
High
RNA Expression
High B7-H6
B7-H6
RNA Expression
Cell Barcode Read Counts
c
Negative
Low
Medium
High
HLA-A/B/C Protein Scores
B2M
HLA-A
HLA-B
HLA-C
HLA-E
Low HLA-A/B/C
RNA Expression
FITC-A
SSC-A
HLA-A/B/C labeled cells
Unlabeled
d
B7-H6
P=0.002, X² test
AUC
Protein Scores
High B7-H6
HLA-A/B/C
P=0.02, X² test
Low HLA-A/B/C
Median AUC
HLA-A/B/C Protein scores
B7-H6 Protein Scores
High B7H6
Low HLA-A/B/C
14
76
25
p=0.0013

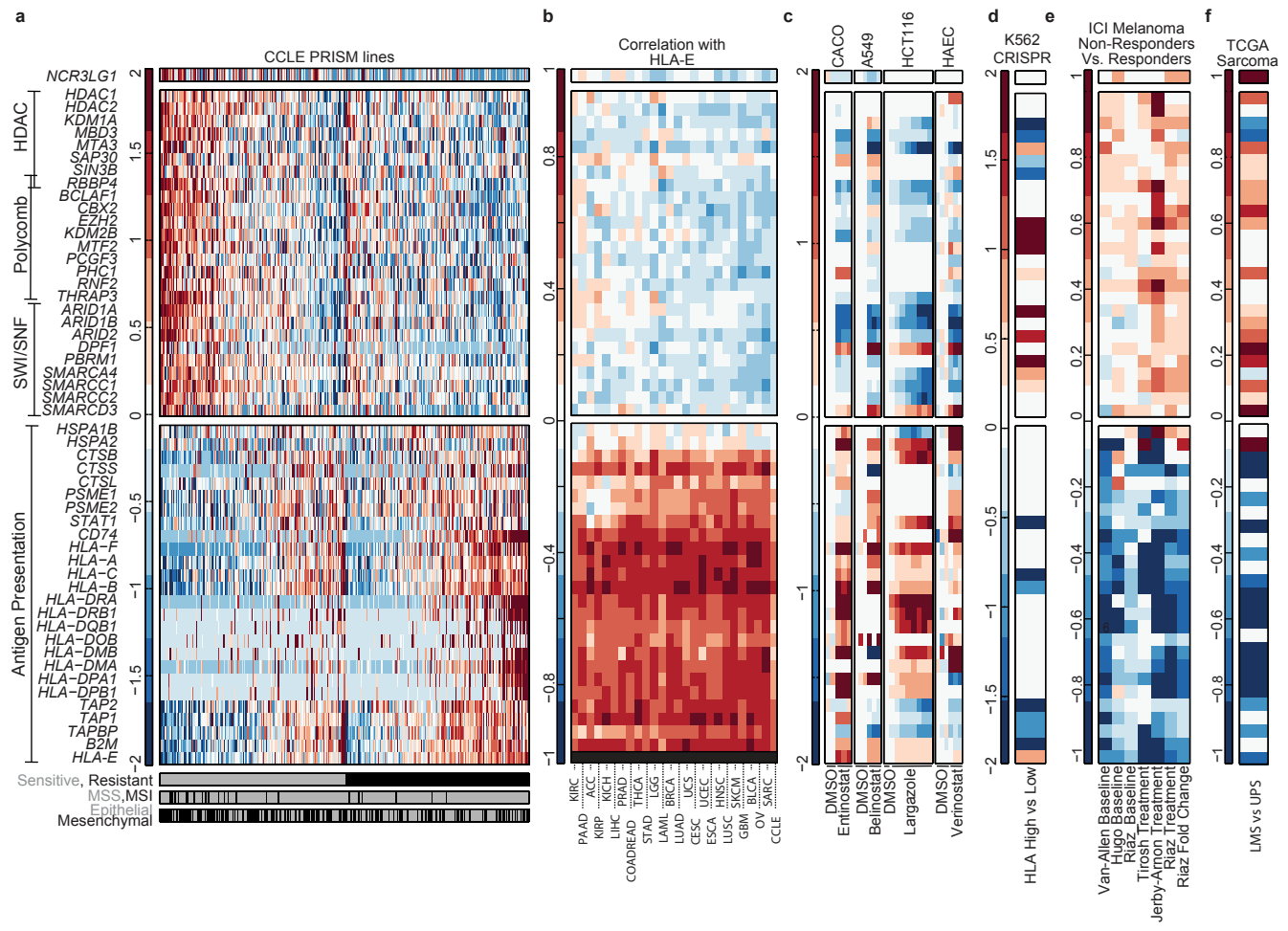
a
CCLE PRISM lines
NCR3LG1
HDAC1
HDAC2
KDM1A
MBD3
MTA3
SAP30
SIN3B
RBBP4
BCLAF1
CBX2
EZH2
KDM2B
MTF2
PCGF3
PHC1
RNF2
THRAP3
ARID1A
ARID1B
ARID2
DPF1
PBRM1
SMARCA4
SMARCC1
SMARCC2
SMARCD3
HSPA1B
HSPA2
CTSB
CTSS
CTSL
PSME1
PSME2
STAT1
CD74
HLA−F
HLA−A
HLA−C
HLA−B
HLA−DRA
HLA−DRB1
HLA−DQB1
HLA−DOB
HLA−DMB
HLA−DMA
HLA−DPA1
HLA−DPB1
TAP2
TAP1
TAPBP
B2M
HLA-E
HDAC
Polycomb
SWI/SNF
Antigen Presentation
Sensitive, Resistant
MSS,MSI
Epithelial
Mesenchymal
b
Correlation with HLA-E
KIRC
PAAD
ACC
KIRP
KICH
LIHC
PRAD
COADREAD
THCA
STAD
LGG
LAML
BRCA
LUAD
UCS
CESC
UCEC
ESCA
HNSC
LUSC
SKCM
GBM
BLCA
OV
SARC
CCLE
c
CACO
A549
HCT116
HAEC
DMSO
Entinostat
DMSO
Belinostat
DMSO
Largazole
DMSO
Verinostat
d
K562 CRISPR
HLA High vs Low
e
ICI Melanoma Non-Responders Vs. Responders
Van-Allen Baseline
Hugo Baseline
Riaz Baseline
Tirosh Treatment
Jerby-Arnon Treatment
Riaz Treatment
Riaz Fold Change
f
TCGA Sarcoma
LMS vs UPS

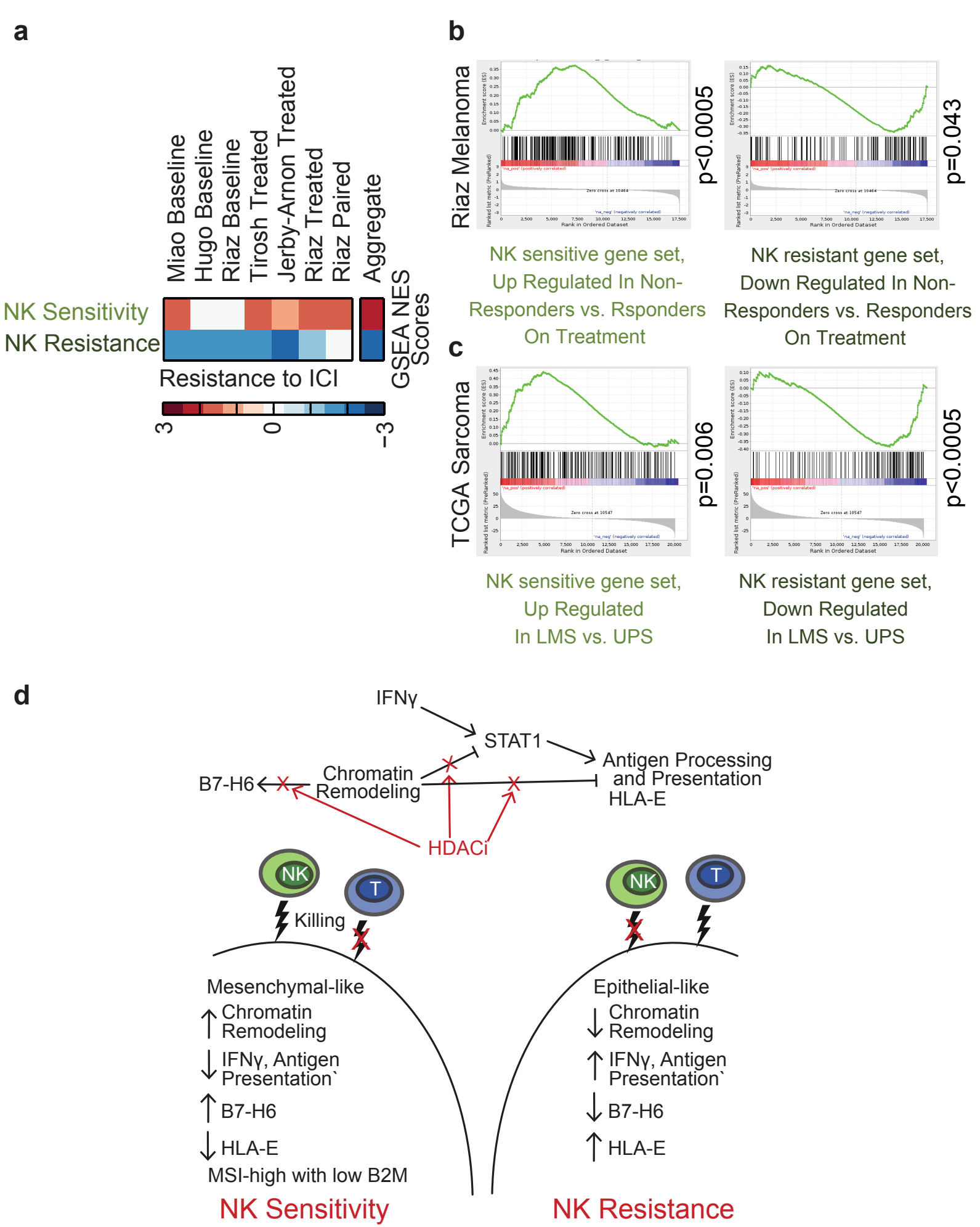
a
Miao Baseline
Hugo Baseline
Riaz Baseline
Tirosh Treated
Jerby-Arnon Treated
Riaz Treated
Riaz Paired
Aggregate
NK Sensitivity
NK Resistance
GSEA NES Scores
Resistance to ICI
3
0
−3
b
Riaz Melanoma
p<0.0005
p=0.043
NK sensitive gene set, Up Regulated In Non-Responders vs. Rsponders On Treatment
NK resistant gene set, Down Regulated In Non-Responders vs. Responders On Treatment
c
TCGA Sarcoma
p=0.006
p<0.0005
NK sensitive gene set, Up Regulated In LMS vs. UPS
NK resistant gene set, Down Regulated In LMS vs. UPS
d
IFNγ
STAT1
Antigen Processing and Presentation HLA-E
B7-H6
Chromatin Remodeling
HDACi
NK
T
Killing
Mesenchymal-like
↑ Chromatin Remodeling
↓ IFNγ, Antigen Presentation`
↑ B7-H6
↓ HLA-E
MSI-high with low B2M
NK Sensitivity
Epithelial-like
↓ Chromatin Remodeling
↑ IFNγ, Antigen Presentation`
↓ B7-H6
↑ HLA-E
NK Resistance

a

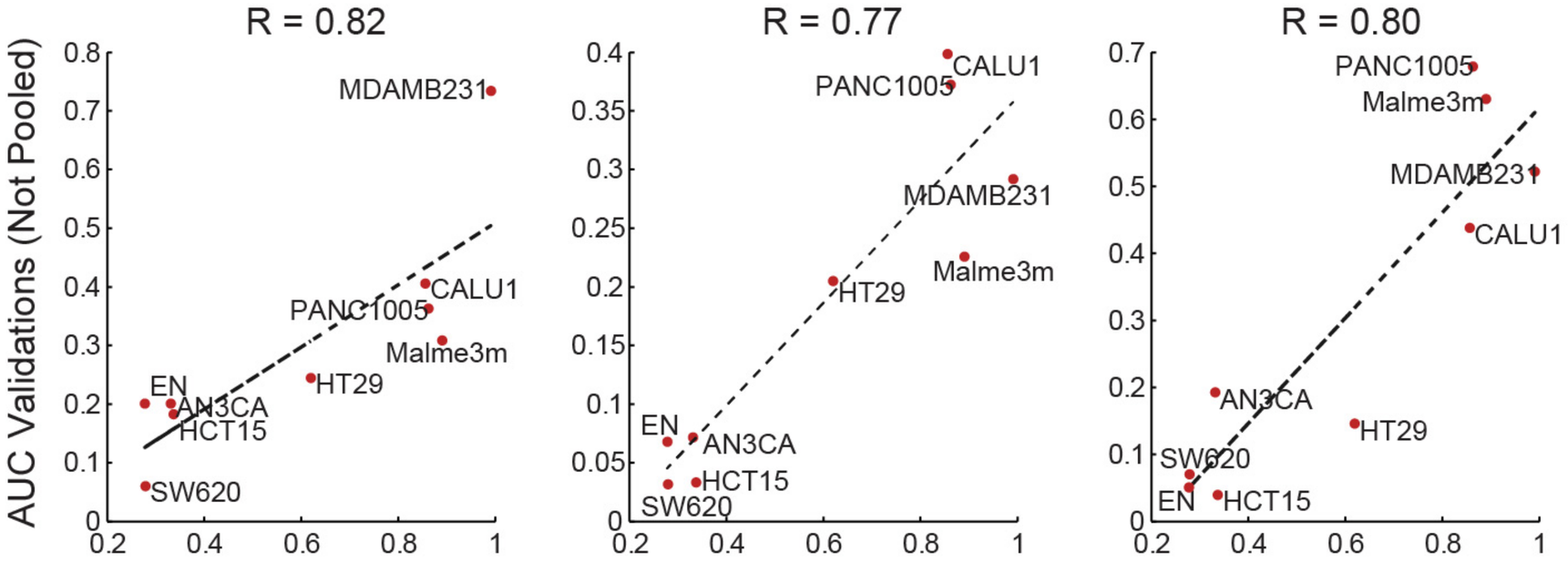
R = 0.82
AUC Validations (Not Pooled)
AUC PRISM, 24hr
MDAMB231
CALU1
PANC1005
Malme3m
HT29
EN
AN3CA
HCT15
SW620
R = 0.77
AUC PRISM, 48hr
CALU1
PANC1005
MDAMB231
Malme3m
HT29
EN
AN3CA
HCT15
SW620
R = 0.80
AUC PRISM, 72hr
PANC1005
Malme3m
MDAMB231
CALU1
AN3CA
HT29
SW620
EN
HCT15

b

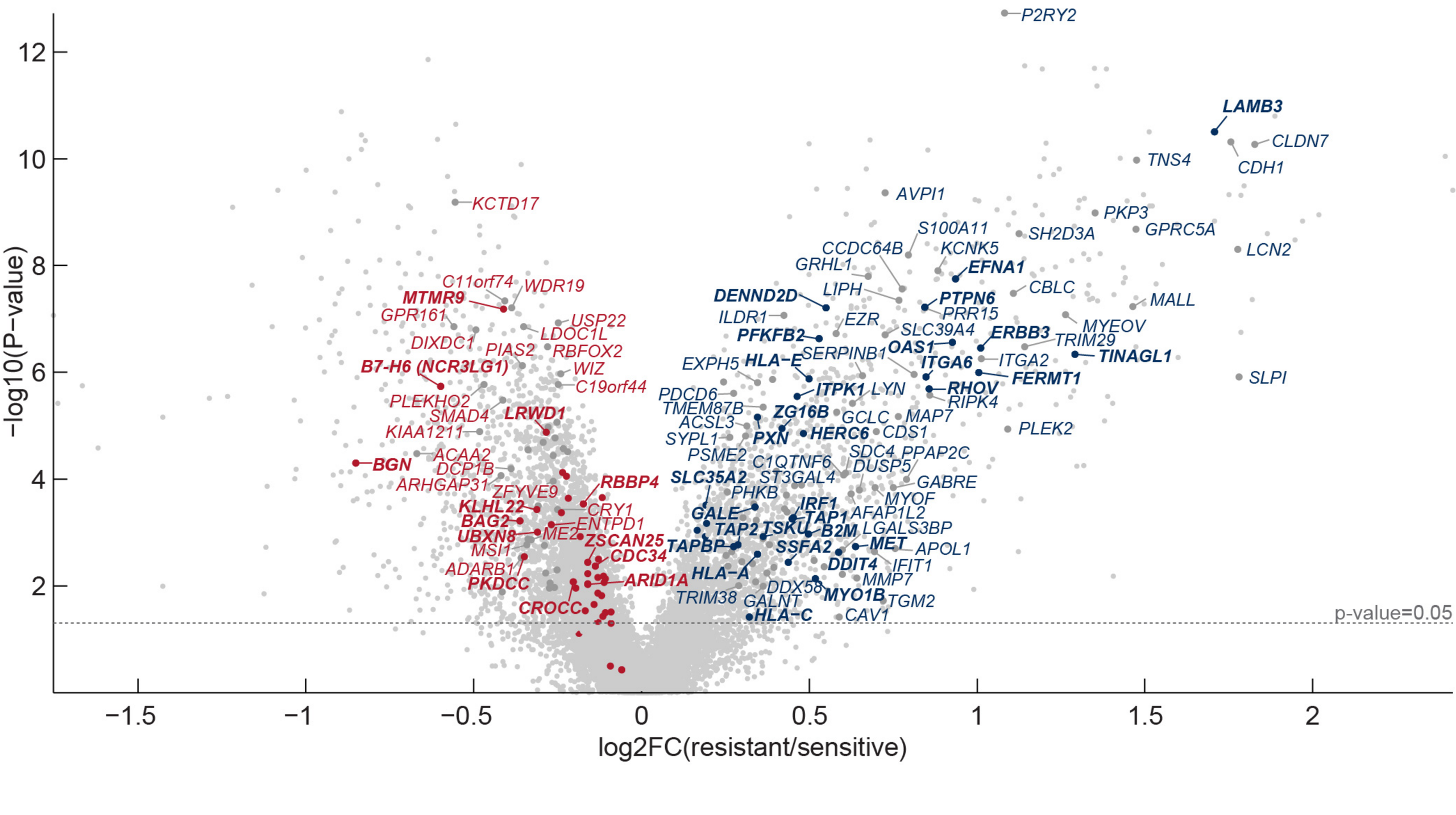
−log10(P−value)
log2FC(resistant/sensitive)
p-value=0.05
P2RY2
LAMB3
CLDN7
CDH1
TNS4
AVPI1
PKP3
GPRC5A
S100A11
SH2D3A
LCN2
CCDC64B
KCNK5
GRHL1
EFNA1
CBLC
MALL
DENND2D
LIPH
PTPN6
PRR15
ILDR1
EZR
SLC39A4
ERBB3
MYEOV
TRIM29
PFKFB2
OAS1
TINAGL1
EXPH5
HLA−E
SERPINB1
ITGA6
ITGA2
FERMT1
SLPI
PDCD6
ITPK1
LYN
RHOV
RIPK4
TMEM87B
ZG16B
GCLC
MAP7
ACSL3
PXN
HERC6
CDS1
PLEK2
SYPL1
PSME2
C1QTNF6
SDC4
PPAP2C
DUSP5
SLC35A2
ST3GAL4
GABRE
PHKB
MYOF
IRF1
GALE
TAP1
AFAP1L2
TAP2
TSKU
B2M
LGALS3BP
TAPBP
SSFA2
MET
APOL1
DDIT4
IFIT1
HLA−A
MMP7
DDX58
MYO1B
TRIM38
GALNT
TGM2
HLA−C
CAV1
KCTD17
C11orf74
WDR19
MTMR9
GPR161
USP22
LDOC1L
DIXDC1
PIAS2
RBFOX2
B7-H6 (NCR3LG1)
WIZ
C19orf44
PLEKHO2
SMAD4
LRWD1
KIAA1211
ACAA2
BGN
DCP1B
ARHGAP31
ZFYVE9
RBBP4
KLHL22
CRY1
BAG2
ENTPD1
UBXN8
ME2
ZSCAN25
MSI1
CDC34
ADARB1
ARID1A
PKDCC
CROCC

sgRNA Enrichment in HT29

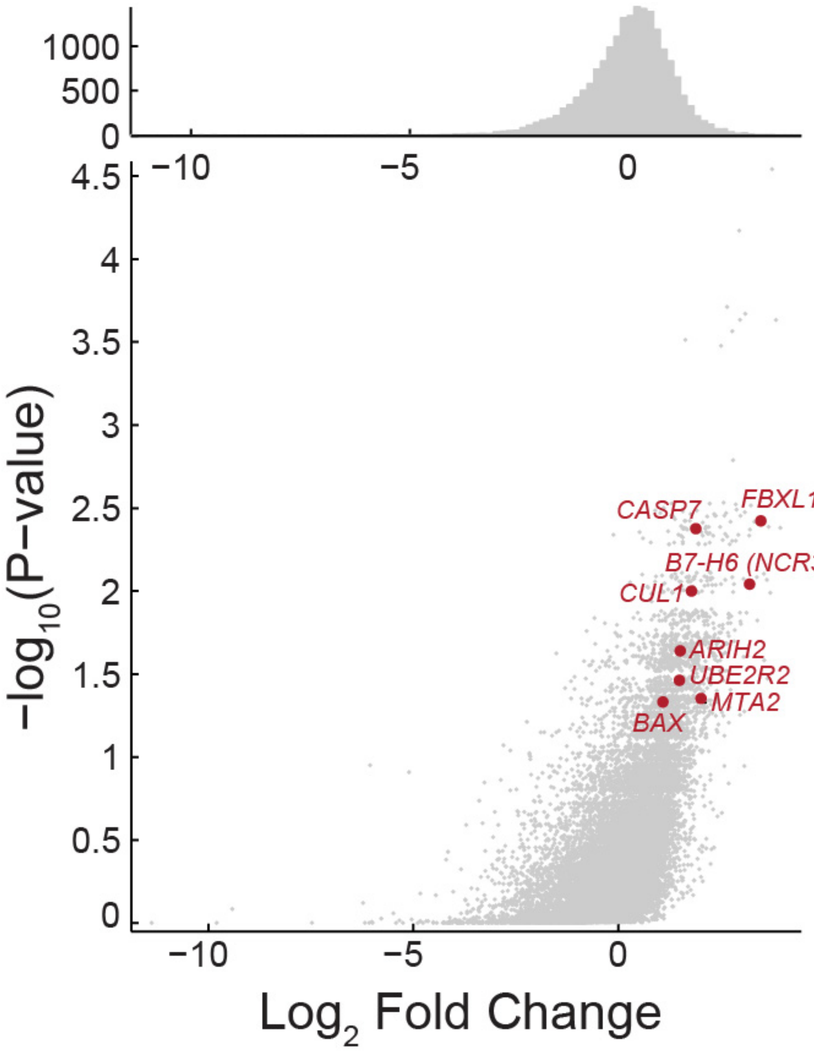

sgRNA Enrichment in SW620

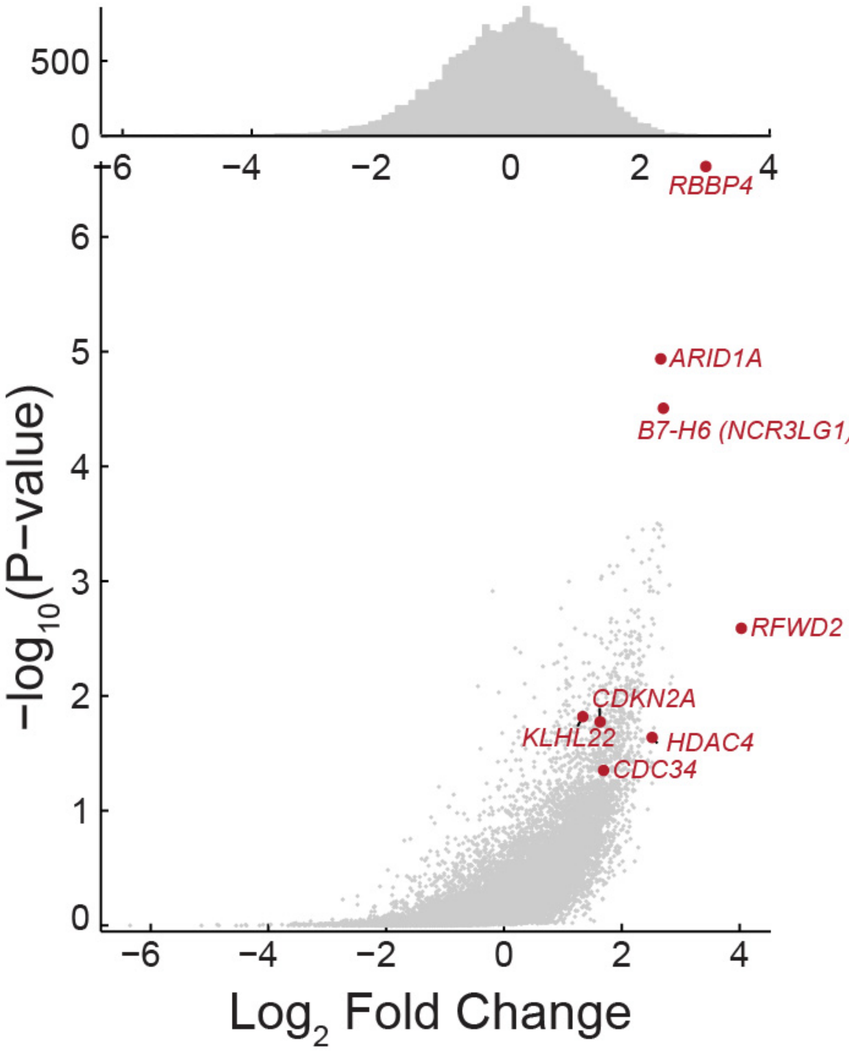

sgRNA Enrichment in HCT15

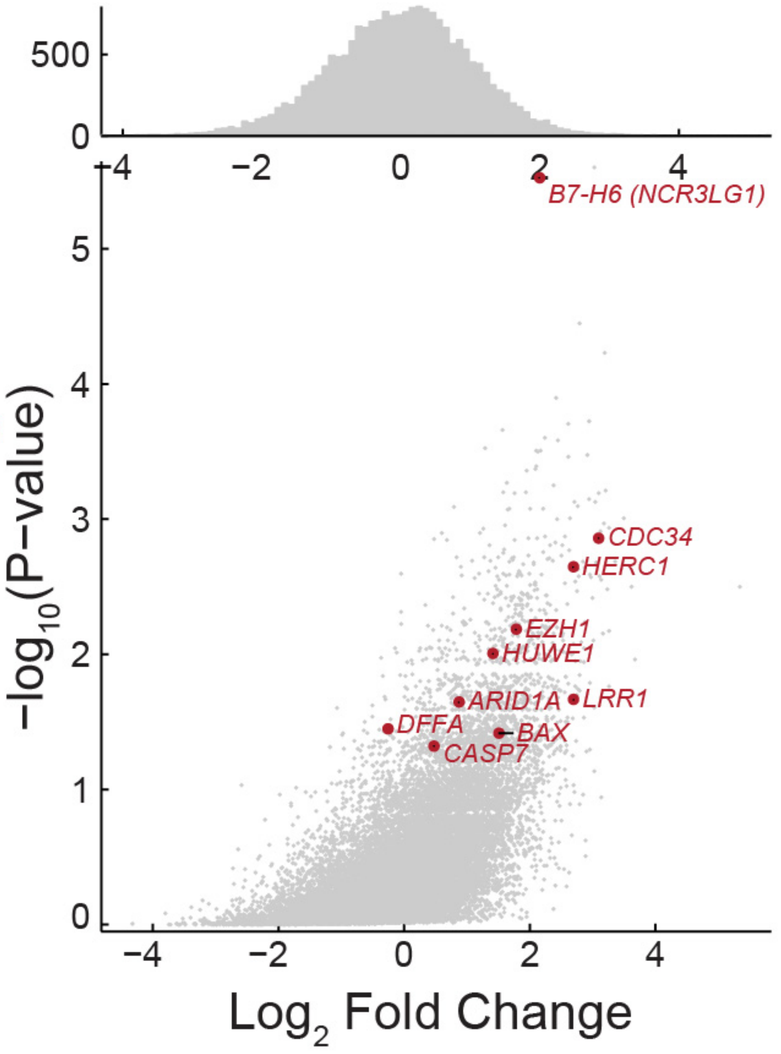

sgRNA depletion in HT29

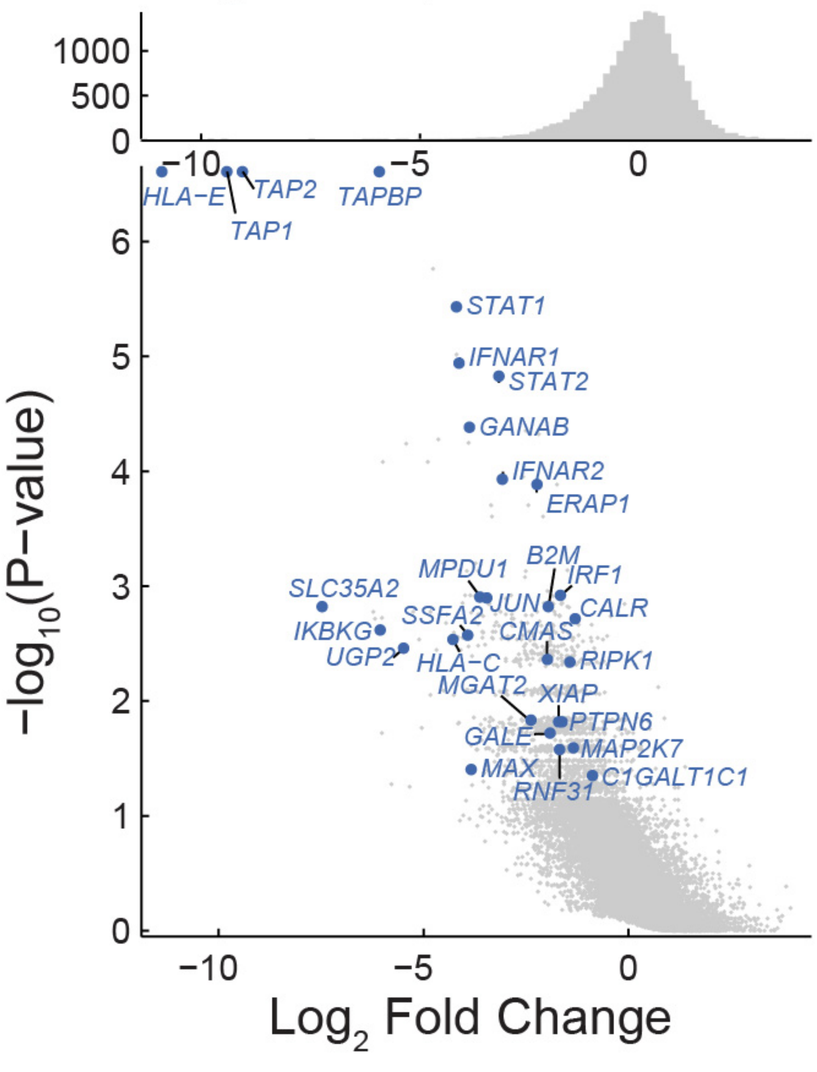

sgRNA depletion in SW620

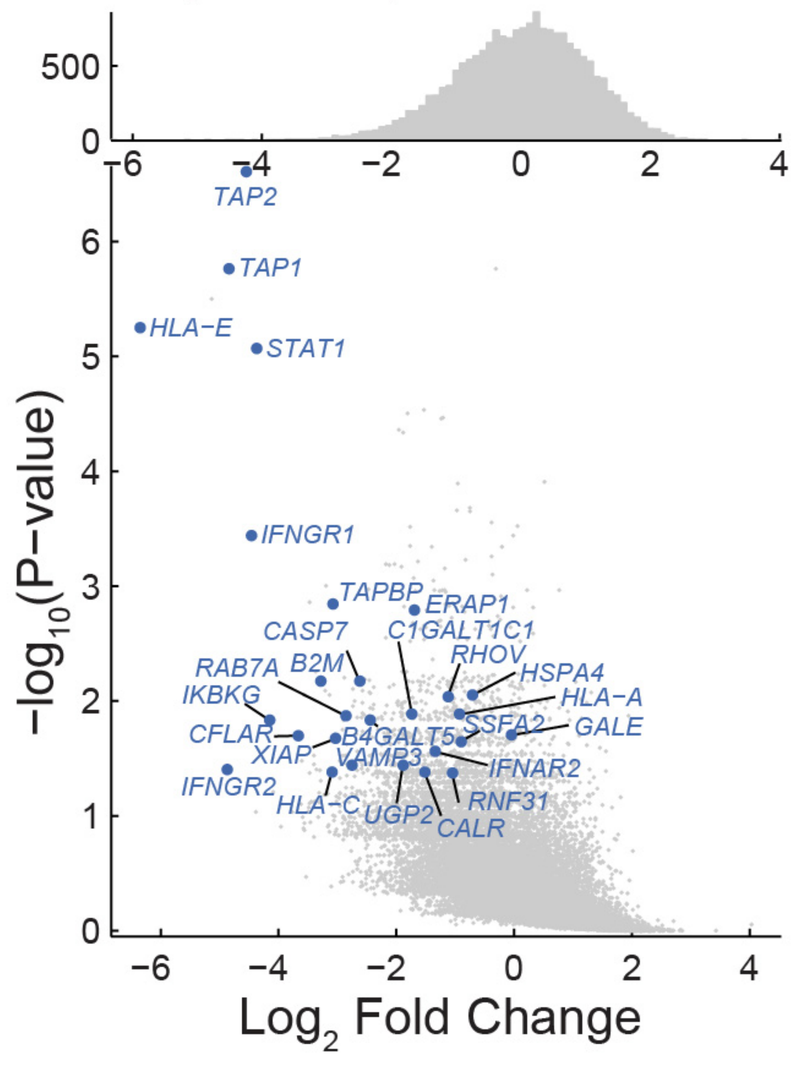

sgRNA depletion in HCT15

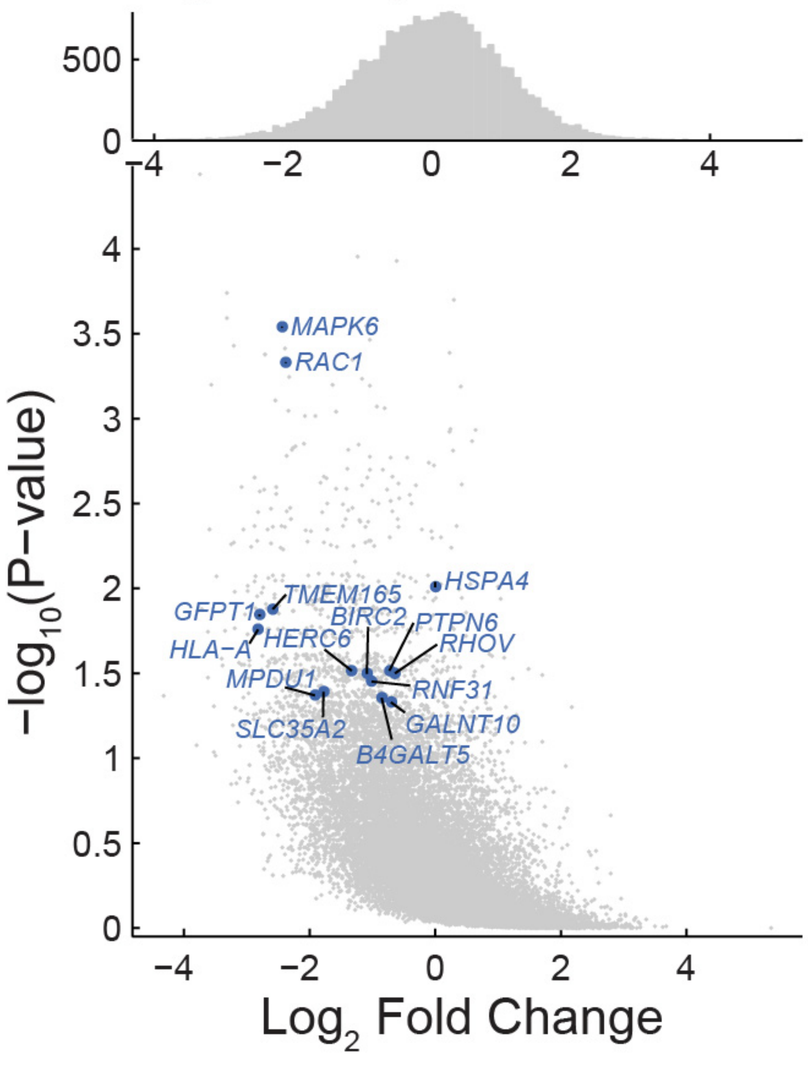

Global Analysis (All Cells)

Epithelial−Like Lines Only

Mesenchymal−Like Lines Only

Genes

2
1.5
1
0.5
0
−0.5
−1
−1.5
−2

500
1000
1500
2000
2500
3000

A Correlated in all analyses (Global Analysis, Epithelial-Like, Mesenchymal-Like)

B Correlated in Global Analysis and in Epithelial-Like

C Correlated in Global Analysis and in Mesenchymal-Like

D Correlated in Global Analysis

Sensitive, Resistant Lines

Antigen Presentation MHC class I

B2M
CALR
HLA-A
HLA-C
HLA-E
TAP1
TAP2
TAPBP
ERAP1
HSPA4

Interferon Response/ Toll-like Receptor Signaling

STAT1
IFNAR1
IFNAR2
IKBKG
RIPK1
JUN
MAP2K7
PTPN6
RNF31
RAC1
STAT2
IFNGR1
IFNGR2
IRF1
HERC6

NK Ligands

NCR3LG1
HLA-A
HLA-C
HLA-E

Amino-Sugar Metabolism

UGP2
GALE
GFPT1
CMAS
SLC35A2

Glycosylation

B4GALT5
C1GALT1C1
GALNT10
MPDU1
MGAT2
GFPT1
TMEM165
GANAB

MAPK/ Ras Signaling

RAC1
STAT1
RIPK1
JUN
MAP2K7
MAX
MAPK6
RHOV
SSFA2

Apoptosis

CASP7
BAX
DFFA
CDKN2A
RIPK1
CFLAR
BIRC2
XIAP

E3-Ligase Ubiquitination

RFWD2
ARIH2
HUWE1
CUL1
CDC34
FBXL12
KLHL22
UBE2R2
HERC1
LRR1

Chromatin Remodeling

MBTD1
EZH1
MTA2
RBBP4
ARID1A
HDAC4

sgRNA depletion in CRISPR
sgRNA enrichment in CRISPR

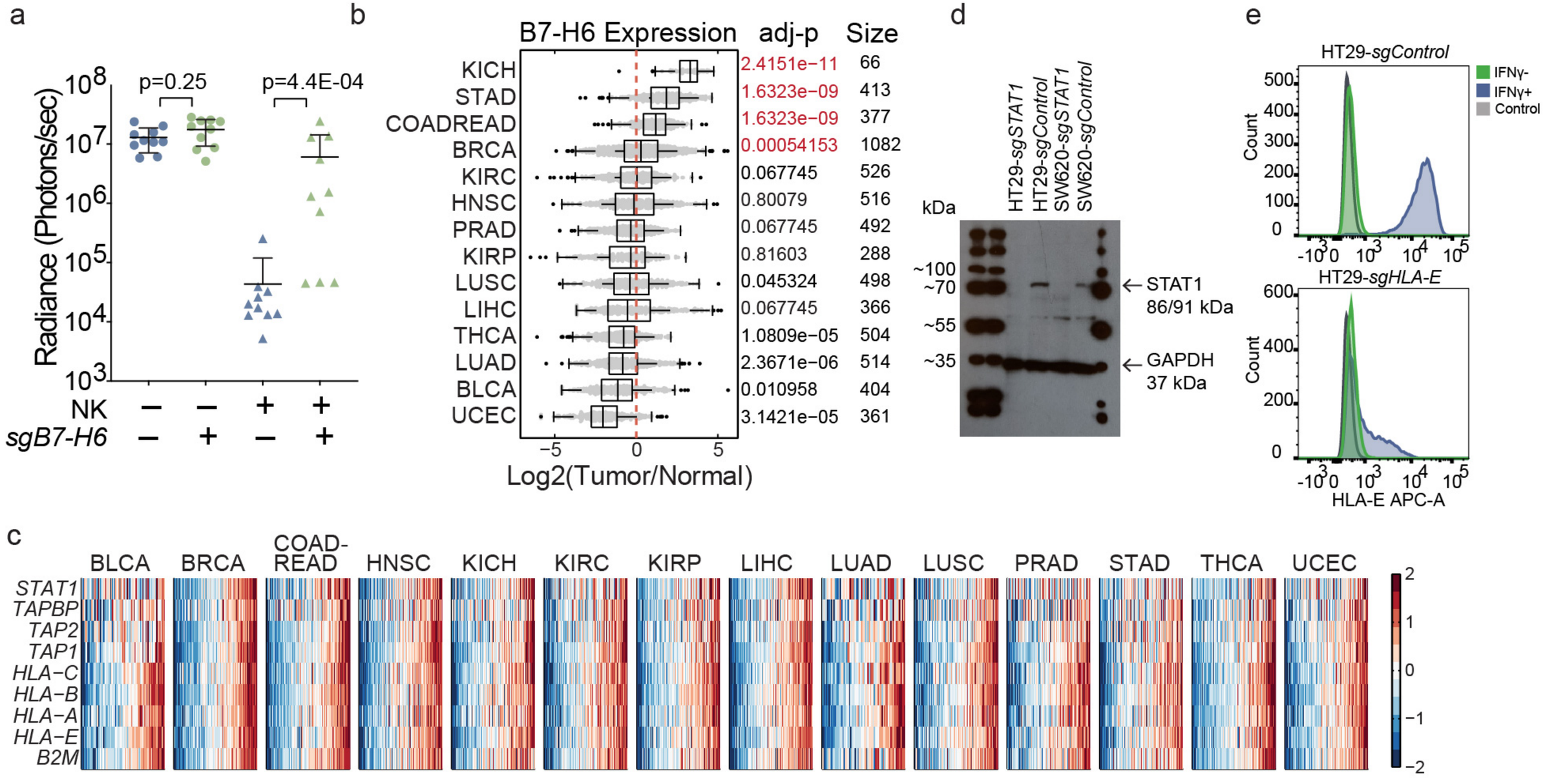
a
Radiance (Photons/sec)
p=0.25
p=4.4E-04
NK
sgB7-H6
b
B7-H6 Expression
adj-p
Size
KICH 2.4151e−11 66
STAD 1.6323e−09 413
COADREAD 1.6323e−09 377
BRCA 0.00054153 1082
KIRC 0.067745 526
HNSC 0.80079 516
PRAD 0.067745 492
KIRP 0.81603 288
LUSC 0.045324 498
LIHC 0.067745 366
THCA 1.0809e−05 504
LUAD 2.3671e−06 514
BLCA 0.010958 404
UCEC 3.1421e−05 361
Log2(Tumor/Normal)
c
BLCA
BRCA
COAD-READ
HNSC
KICH
KIRC
KIRP
LIHC
LUAD
LUSC
PRAD
STAD
THCA
UCEC
STAT1
TAPBP
TAP2
TAP1
HLA−C
HLA−B
HLA−A
HLA−E
B2M
d
HT29-sgSTAT1
HT29-sgControl
SW620-sgSTAT1
SW620-sgControl
kDa
~100
~70
~55
~35
STAT1 86/91 kDa
GAPDH 37 kDa
e
HT29-sgControl
HT29-sgHLA-E
IFNγ-
IFNγ+
Control
Count
HLA-E APC-A

a

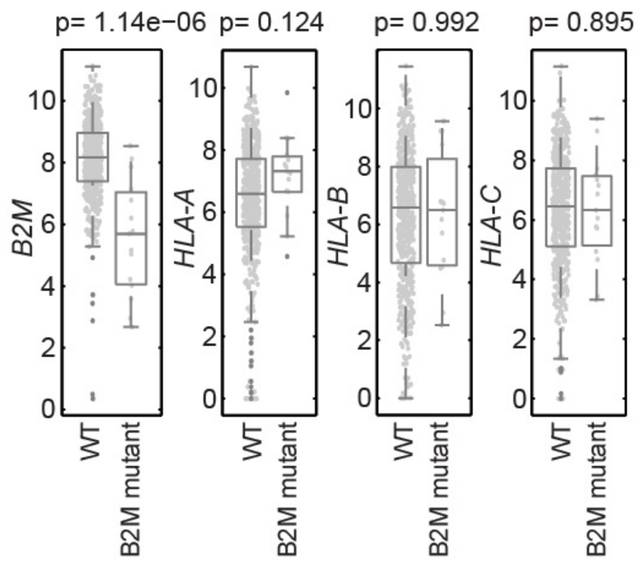
p= 1.14e−06
p= 0.124
p= 0.992
p= 0.895
B2M
HLA-A
HLA-B
HLA-C
WT
B2M mutant

b

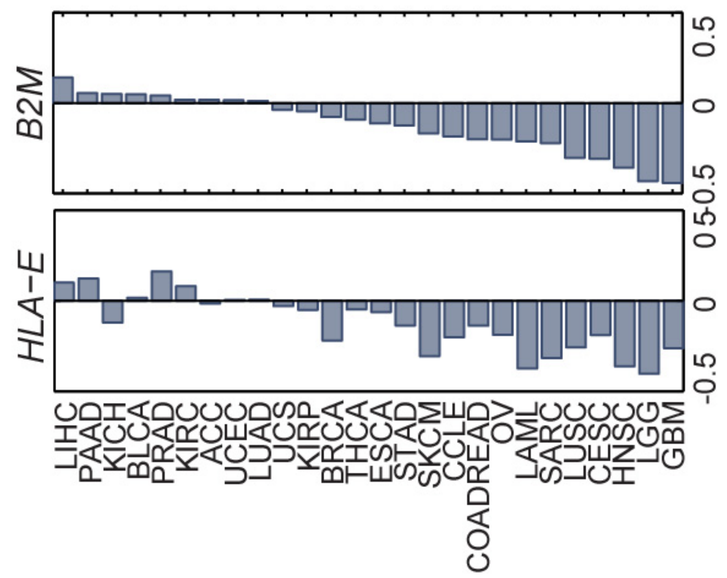
B2M
HLA−E
LIHC
PAAD
KICH
BLCA
PRAD
KIRC
ACC
UCEC
LUAD
UCS
KIRP
BRCA
THCA
ESCA
STAD
SKCM
CCLE
COADREAD
OV
LAML
SARC
LUSC
CESC
HNSC
LGG
GBM

c

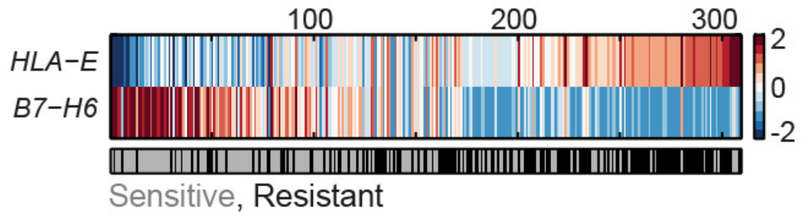
HLA−E
B7−H6
Sensitive, Resistant

d

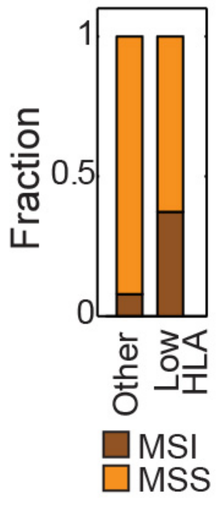
Fraction
Other
Low HLA
MSI
MSS

e

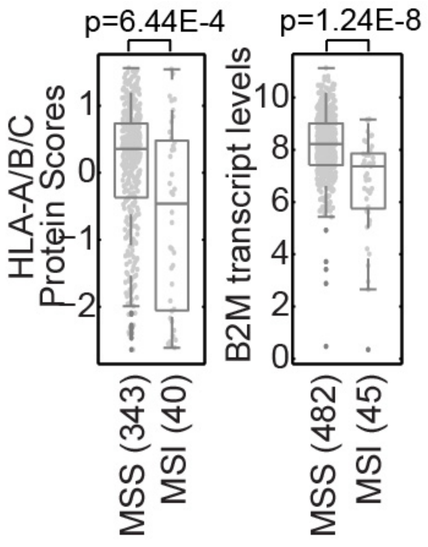
p=6.44E-4
p=1.24E-8
HLA-A/B/C Protein Scores
B2M transcript levels
MSS (343)
MSI (40)
MSS (482)
MSI (45)

f

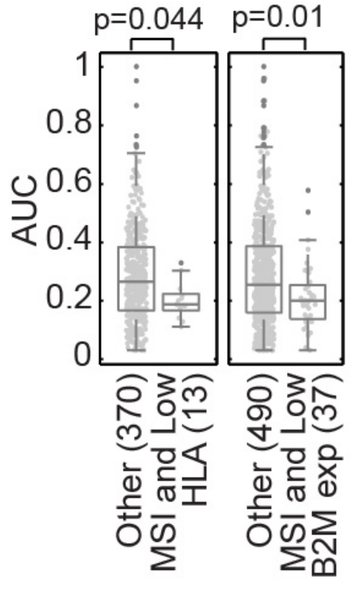
p=0.044
p=0.01
AUC
Other (370)
MSI and Low HLA (13)
Other (490)
MSI and Low B2M exp (37)

g

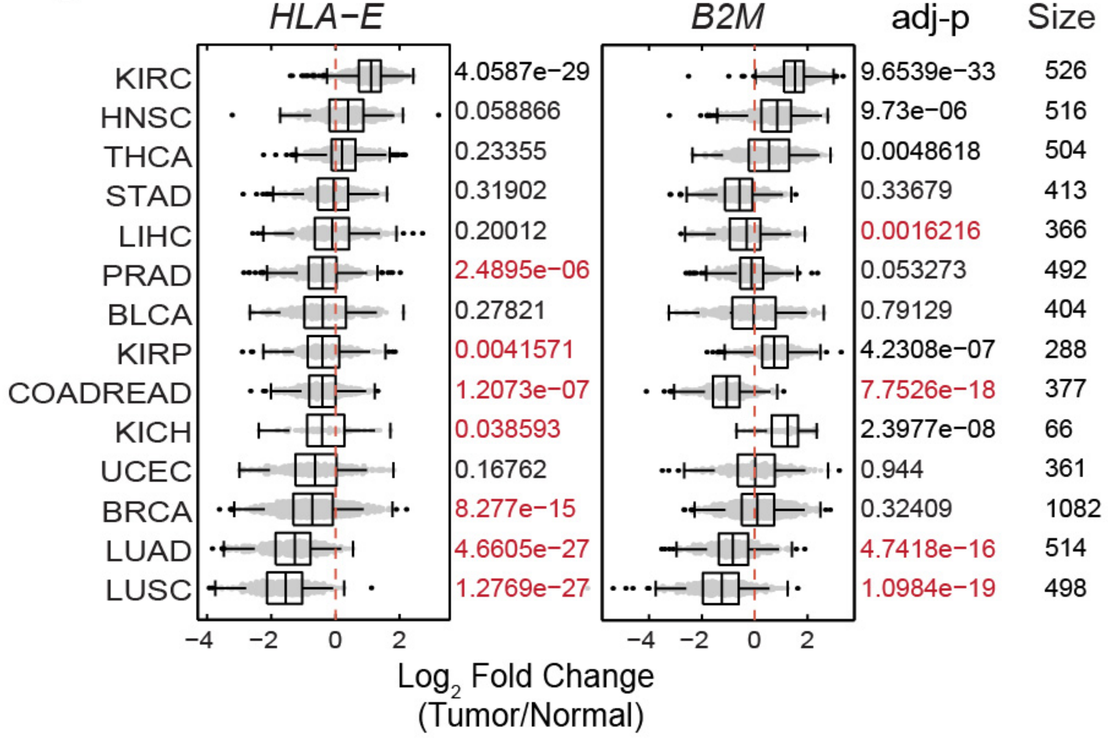
HLA−E
B2M
adj-p
Size
KIRC 4.0587e−29 9.6539e−33 526
HNSC 0.058866 9.73e−06 516
THCA 0.23355 0.0048618 504
STAD 0.31902 0.33679 413
LIHC 0.20012 0.0016216 366
PRAD 2.4895e−06 0.053273 492
BLCA 0.27821 0.79129 404
KIRP 0.0041571 4.2308e−07 288
COADREAD 1.2073e−07 7.7526e−18 377
KICH 0.038593 2.3977e−08 66
UCEC 0.16762 0.944 361
BRCA 8.277e−15 0.32409 1082
LUAD 4.6605e−27 4.7418e−16 514
LUSC 1.2769e−27 1.0984e−19 498
Log2 Fold Change
(Tumor/Normal)

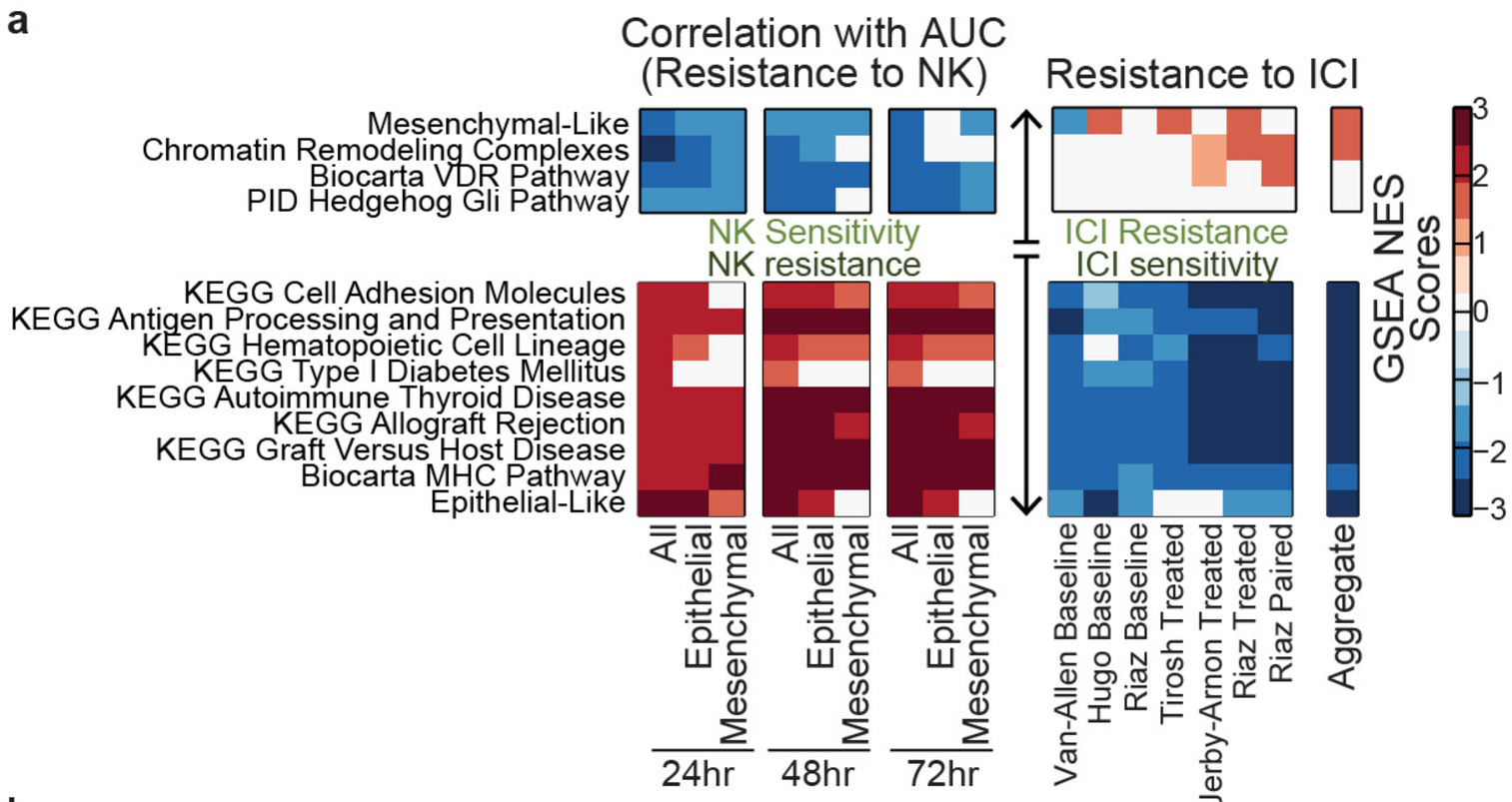
a
Correlation with AUC
(Resistance to NK)
Resistance to ICI
Mesenchymal-Like
Chromatin Remodeling Complexes
Biocarta VDR Pathway
PID Hedgehog Gli Pathway
NK Sensitivity
NK resistance
ICI Resistance
ICI sensitivity
KEGG Cell Adhesion Molecules
KEGG Antigen Processing and Presentation
KEGG Hematopoietic Cell Lineage
KEGG Type I Diabetes Mellitus
KEGG Autoimmune Thyroid Disease
KEGG Allograft Rejection
KEGG Graft Versus Host Disease
Biocarta MHC Pathway
Epithelial-Like
All
Epithelial
Mesenchymal
24hr
48hr
72hr
Van-Allen Baseline
Hugo Baseline
Riaz Baseline
Tirosh Treated
Jerby-Arnon Treated
Riaz Treated
Riaz Paired
Aggregate
GSEA NES Scores
3
2
1
0
−1
−2
−3

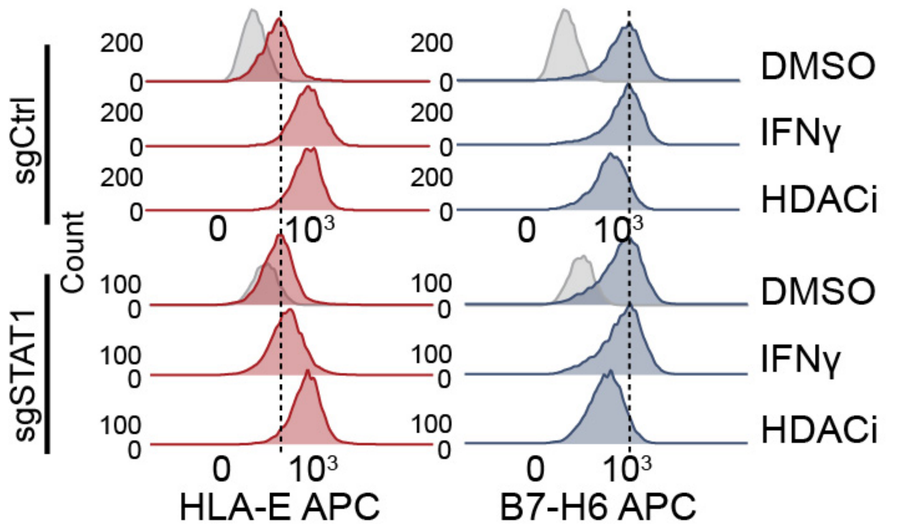
d
sgCtrl
sgSTAT1
Count
200
100
0
10^3
DMSO
IFNγ
HDACi
HLA-E APC
B7-H6 APC

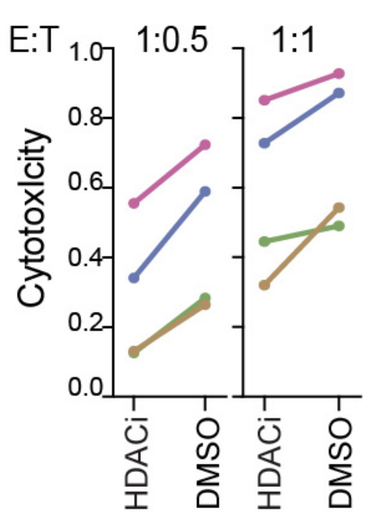
e
E:T
1:0.5
1:1
Cytotoxicity
1.0
0.8
0.6
0.4
0.2
0.0
HDACi
DMSO

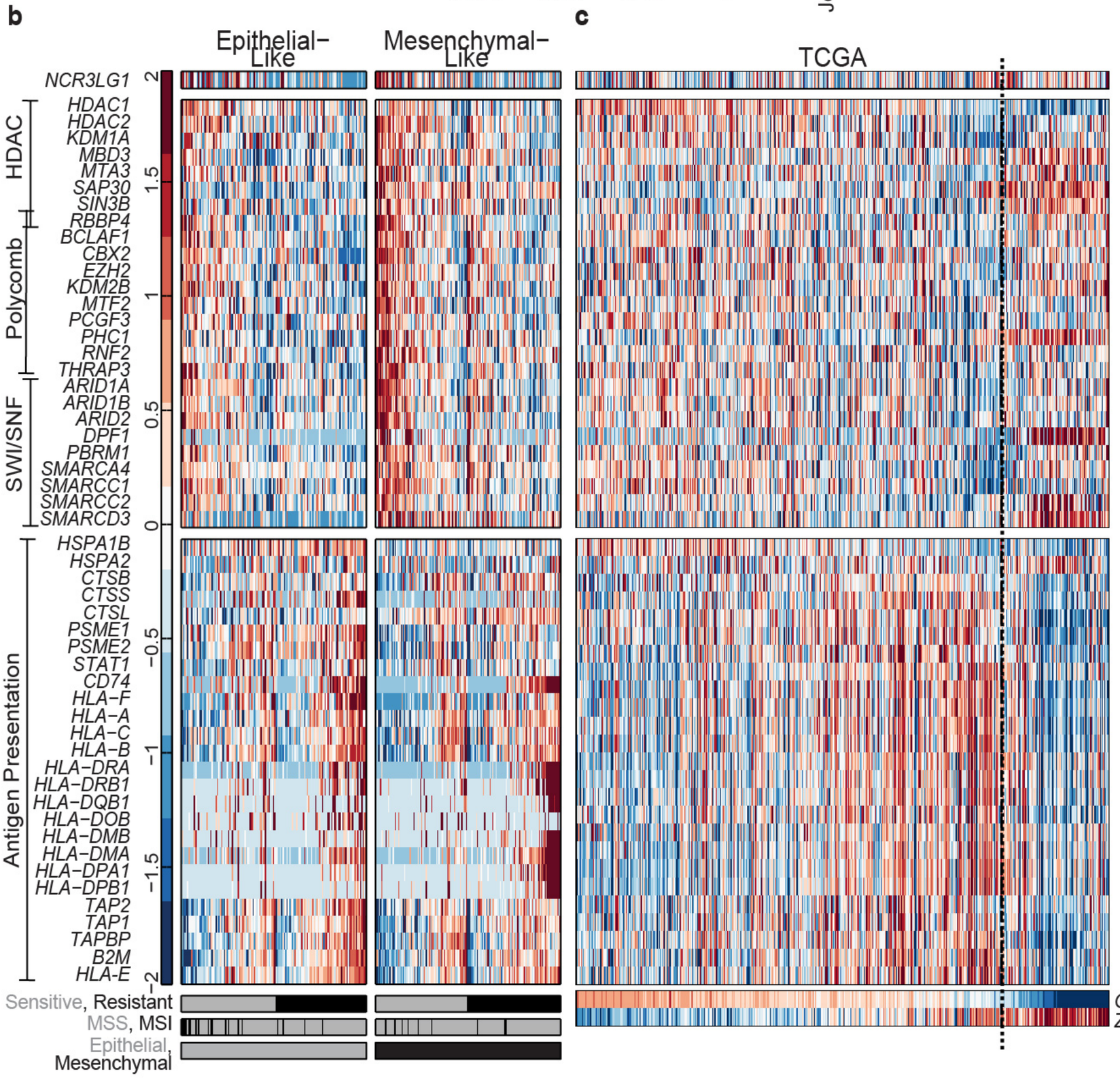
b
c
Epithelial-Like
Mesenchymal-Like
TCGA
NCR3LG1
HDAC
HDAC1
HDAC2
KDM1A
MBD3
MTA3
SAP30
SIN3B
RBBP4
Polycomb
BCLAF1
CBX2
EZH2
KDM2B
MTF2
PCGF3
PHC1
RNF2
THRAP3
SWI/SNF
ARID1A
ARID1B
ARID2
DPF1
PBRM1
SMARCA4
SMARCC1
SMARCC2
SMARCD3
Antigen Presentation
HSPA1B
HSPA2
CTSB
CTSS
CTSL
PSME1
PSME2
STAT1
CD74
HLA-F
HLA-A
HLA-C
HLA-B
HLA-DRA
HLA-DRB1
HLA-DQB1
HLA-DOB
HLA-DMB
HLA-DMA
HLA-DPA1
HLA-DPB1
TAP2
TAP1
TAPBP
B2M
HLA-E
2
1.5
1
0.5
0
−0.5
−1
−1.5
−2
Sensitive, Resistant
MSS, MSI
Epithelial, Mesenchymal
CDH1
ZEB2

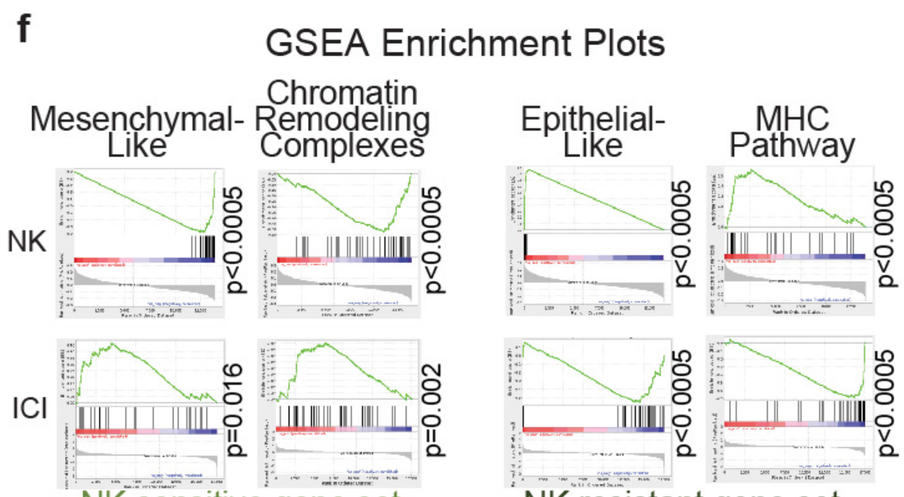
f
GSEA Enrichment Plots
Mesenchymal-Like
Chromatin Remodeling Complexes
Epithelial-Like
MHC Pathway
NK
ICI
p<0.0005
p=0.016
p=0.002
NK sensitive gene set, Up Regulated In Non-Responders vs. Responders On Treatment
NK resistant gene set, Down Regulated In Non-Responders vs. Responders On Treatment

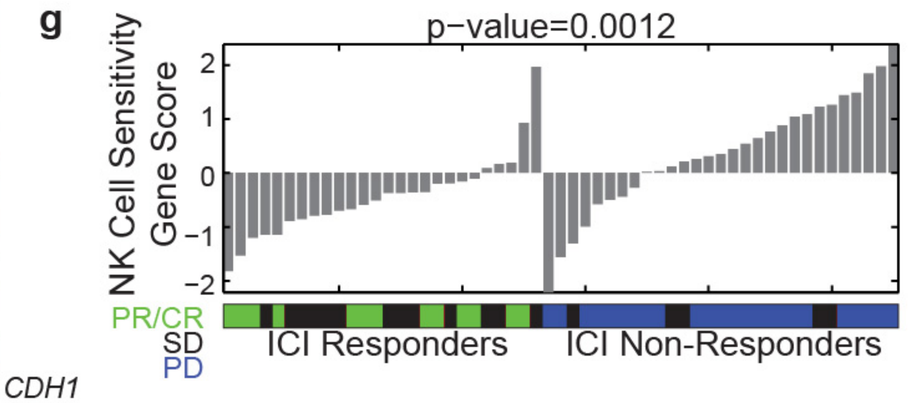
g
p−value=0.0012
NK Cell Sensitivity Gene Score
2
1
0
−1
−2
PR/CR
SD
PD
ICI Responders
ICI Non-Responders